Recently, organic anion transporting polypeptide 14 (Oatp14; *Slc21a14*) has been cloned from the rat brain cDNA library using gene microarray techniques by comparing the gene-expression profile of cDNA from the brain capillary with that from the liver and kidney (10). Oatp14 was highly enriched in the brain capillary, compared with brain homogenate, liver, and kidney (10, 11). Functional expression of OATP-F, the human ortholog of Oatp14, revealed that T_4 and the inactive metabolite, rT_3, are high-affinity substrates (12), and rOatp14 accepts amphipathic organic anions, such as cerivastatin, 17β-estradiol-D-17β-glucuronide ($E_2$17βG), and troglitazone sulfate as substrates in addition to T_4 and rT_3 (11). The transport activity of T_3 by OATP-F and rOatp14 was small, compared with that of T_4 and rT_3. Because the expression level of rOatp14 is controlled by the plasma thyroid hormone concentrations (11), it has been hypothesized that rOatp14 is involved in the uptake of thyroid hormones by the brain. There are additional candidate transporters for the transport of thyroid hormones at the brain: Oatp2, another isoform of the Oatp family, large neutral amino acid transporters, and monocarboxylate transporter 8 (MCT8) (13–17). The present study is aimed at investigating whether mOatp14 is involved in the brain uptake of T_4 across the BBB. Stable transformants of mOatp14 were established to reveal the spectrum of inhibitors. The *in situ* brain perfusion technique was carried out to investigate the uptake of T_4 across the BBB, and the effect of inhibitors for mOatp14, Oatp2, and neutral amino acid transporter was examined to reveal the contribution of mOatp14.

Materials and Methods

Chemicals

L-[^{125}I]T_4, [^{3}H]$E_2$17βG, [^{3}H]estrone-3-sulfate (E-sul), [^{125}I]rT_3, and [^{125}I]T_3 were purchased from PerkinElmer Life Science (Boston, MA). [^{14}C]sucrose was purchased from Moravek Biochemicals (Brea, CA). All other chemicals and reagents were of analytical grade and readily available from commercial sources. Before the experiments the purity check of labeled T_4, T_3, and rT_3 was performed using HPLC. HPLC conditions were as follows: column, HPLC column (4 mm; YMC, Kyoto, Japan), 4.6 mm inner diameter × 15 cm; mobile phase 0.2% phosphate buffer/methanol (50/50); rate, 1 ml/min; column temperature, 30 C (18). T_4, T_3, rT_3, and 3,5-T_2 can separate under these conditions.

Animals

Adult male ddY mice (28–35 g, 7–8 wk old) were obtained from Japan SLC, Inc (Shizuoka, Japan). All the animals used throughout this study had free access to food and water. The animal experiments were approved by the Institution Animal Care Committee (Graduate School of Pharmaceutical Science, The University of Tokyo), and performed according to its guidelines.

Cloning of mouse Oatp14 (mOatp14) cDNA and construction of a stable transfectant

Based on the nucleotide sequence reported by Okazaki *et al.* (GenBank accession no. NM_021471), the cDNA encoding a full open reading frame of mOatp14 was cloned from mouse brain cDNA using PCR. The mOatp14 cDNA was subcloned into pcDNA3.1(+) (Invitrogen, Carlsbad, CA) and transfected into HEK293 cells by lipofection with FuGENE6 (Roche Diagnostics, Basel, Switzerland) according to the manufacturer's protocol. The transfectants were selected by culturing them in the presence of G418 sulfate (800 μg/ml) (Gibco BRL, Gaithersburg, MD). The transfectants were maintained in DMEM (Gibco) supplemented with 10% fetal bovine serum, 1% antibiotic-antimycotic (Gibco), and G418 sulfate (400 μg/ml) at 37 C with 5% CO_2 and 95% humidity.

Transport study

Uptake was initiated by adding the radiolabeled ligands to the incubating buffer in the presence and absence of inhibitors after cells had been washed twice and preincubated with Krebs-Henseleit buffer at 37 C for 15 min. The Krebs-Hensleit buffer consisted of 23.8 $NaHCO_3$, 118 NaCl, 4.83 KCl, 1.2 $MgSO_4$, 0.96 KH_2PO_4, 1.53 $CaCl_2$, 5 D-glucose, and 12.5 HEPES (millimoles) adjusted to pH 7.4. The uptake was terminated at designated times by adding ice-cold buffer, and cells were washed three times. The radioactivity associated with cell and medium specimens was determined in a liquid scintillation counter and γ-counter. Ligand uptake is given as the cell-to-medium concentration ratio determined as the amount of ligand associated with the cells divided by the medium concentration. Specific uptake was obtained by subtracting the uptake of vector-transfected cells from that by mOatp14-HEK.

In situ brain perfusion

In situ brain perfusion was carried out according the previous report by Dagenais *et al.* (19). Briefly, mice were anesthetized by ip injection of pentobarbital sodium (50 mg/kg), and the right common carotid artery was catheterized with polyethylene tubing (0.2 mm inner diameter × 0.5 mm outer diameter) mounted on a 30-gauge needle. Before insertion of the catheter, the common carotid artery was ligated caudally. During surgery, body temperature was maintained with a heated plate. The syringe containing the perfusion fluid was placed in an infusion pump (Packard Instruments, Meriden, CT) and connected to the catheter. Before perfusion, the thorax of the animal was opened, the heart was cut, and perfusion was started immediately at a flow rate of 1.0 ml/min. The perfusion fluid consisted of Krebs-Henseleit bicarbonate buffer (millimoles): 25 $NaHCO_3$, 118 NaCl, 4.7 KCl, 1.2 $MgSO_4 \cdot 7H_2O$, 1.2 $NaH_2PO_4 \cdot 2H_2O$, 1.2 $CaCl_2 \cdot 2H_2O$, and 10 D-glucose. The perfusion was gassed with 95% O_2 and 5% CO_2 for pH control (7.4) and warmed to 37 C in a water bath. The perfusate contained a vascular space marker ([^{14}C]sucrose) of 2 μCi/ml and perfusion was terminated by decapitation of a number of the animals at selected times. The brain was removed, and the cortex of the right cerebral hemisphere was placed in a tared vial and weighed. The radioactivity associated with the brain and perfusion fluid specimens was determined in a liquid scintillation counter.

Brain vascular volume was estimated from the tissue distribution of [^{14}C] sucrose, which is known to diffuse very slowly across the BBB, using the following equation:

$$V_{vasc} = X^*/C^*_{perf}$$

where X* [dpm (decay per minute) per gram brain] is the amount of sucrose measured in the right cortex and C^*_{perf} (dpm per minute per microliter) is the concentration of labeled sucrose in the perfusate. The apparent volume of brain distribution (V_{brain}) was calculated from the amount of radioactivity in the right cortex using the following equation:

$$V_{brain} = X_{brain}/C_{perf}$$

where X_{brain} (dpm per gram brain) is the amount of tracer measured in the right cortex and C_{perf} (disintegrations per minute per microliter) is the concentration of labeled tracer in the perfusate. Brain tissue radioactivity was corrected for vascular contamination using the following equation:

$$X_{brain} = X_{tot} - V_{vasc}{}^*C_{perf}$$

where X_{tot} (dpm per gram brain) is the total quantity of tracer measured in the tissue sample.

The initial uptake clearance was calculated from the following equation:

$$CL_{up} = V_{brain}/T$$

where T is the perfusion time (minutes).

Kinetic analysis

Kinetic parameters were obtained from the following (Michaelis-Menten) equation:

$$v = V_{max} * S/(K_m + S)$$

where v is the uptake rate of the substrate (picomoles per minute per milligram protein), S is the substrate concentration in the medium (micromoles), K_m is the Michaelis-Menten constant (micromoles), and V_{max} is the maximum uptake rate (picomoles per minute per milligram protein). The experimental data were fitted to the equation by nonlinear regression analysis with weighting as the reciprocal of the observed values using the MULTI program, and the Damping Gauss Newton method algorithm was used for fitting (20).

Inhibition constants (K_i) for mOatp14-mediated transport were calculated from the following equation assuming competitive inhibition:

$$v_{+inhibitor}/v = 1/(1 + I/K_i)$$

where $v_{+inhibitor}$ is the uptake rate of the substrate inhibited by ligands (picomoles per minute per milligram protein) and I is the inhibitor concentration in the medium (micromoles).

Capillary isolation

The method of capillary isolation was described by Ball *et al.* (21) and Dallaire *et al.* (22). Capillary isolation was performed by using the modified method. Briefly, the cortex was homogenized in 0.32 M sucrose (ratio 1 g brain/20 ml sucrose) using a Polytron homogenizer. The homogenate was centrifuged at 4 C at 2200 × *g* for 10 min, and the resulting pellet was suspended in 25% BSA and centrifuged at 4 C at 2200 × *g* for 10 min. The supernatant was decanted, and the pellet was washed three times with buffer: 10 mM Tris-Cl, 0.5 mM dithiothreitol (pH 7.6). The purity of the brain capillary enrichment fraction was examined by estimating the γ-GTP activity.

Northern blot analysis

A commercially available hybridization blot containing poly A+ RNA from various mouse tissues (mouse MTN blot, CLONTECH, Palo Alto, CA) was used for the Northern blot analysis. A fragment (position numbers 86–841) from mOatp14-ORF was used as a probe. The master blot filter was hybridized in Perfecthyb Plus (Sigma, St. Louis, MO) with the ^{32}P-labeled probe at 68 C according to the manufacturer's instructions. Finally, the filter was washed under high stringency conditions (0.1× saline sodium citrate: 0.15 M NaCl and 0.015 M sodium citrate) and 0.1% sodium dodecyl sulfate at 65 C.

Western blot analysis

Antiserum against the carboxyl-terminal of rat Oatp14 (rOatp14) (11) was available for mOatp14. The specimens were loaded onto a 10% SDS-PAGE with a 3.75% stacking gel. Proteins were electroblotted onto a polyvinylidene difluoride membrane (Pall, Port Washington, NY). The membrane was blocked with Tris-buffer saline containing 0.05% Tween 20 and 3% skimmed milk for 1 h at room temperature. After incubation with the primary antibody, detection was carried out by binding a horseradish peroxidase-labeled antirabbit IgG antibody (Amersham Bioscience, Buckinghamshire, UK). Regional difference of mOatp14 was examined using mouse multiple brain tissue region-specific blots (Geno Technology, St. Louis, MO).

Immunohistochemical staining

Adult mice were perfused with 4% paraformaldehyde/PBS. The cerebrum was isolated and stored in 4% paraformaldehyde/PBS for 2 h at 4 C. Before sectioning, the cerebrum was immersed in 20% sucrose at 4 C. Cryostat sections (10 μm thick) were fixed in methanol at −20 C for 10 min, washed with PBS, and blocked with 1% BSA/PBS at room temperature for 4 h, and then primary antibodies (rabbit anti-rOatp14 serum (1:100 dilution in 1% BSA/PBS) and C219 (1:40 dilution in 1% BSA/PBS) were kept at 4 C for 44 h. For detection of the signals, sections were incubated with secondary antibodies (Alexa Fluor 568 antirabbit IgG and Alexa Fluor 488 antimouse IgG, diluted to 1:200; Molecular Probes, Eugene, OR) for 1 h, and the nucleic acid was simultaneously stained with TO-PRO-3 iodide (Molecular Probes) and mounted in Vectashield mounting medium (Vector Laboratories, Burlingame, CA).

Results

Transport properties of mOatp14

Figure 1, A–E, shows the time profiles of the uptake of [^{125}I]L-T4, [^{125}I]rT_3, [^{3}H]$E_2$17βG, [^{125}I]T_3, and [^{3}H]E-sul by

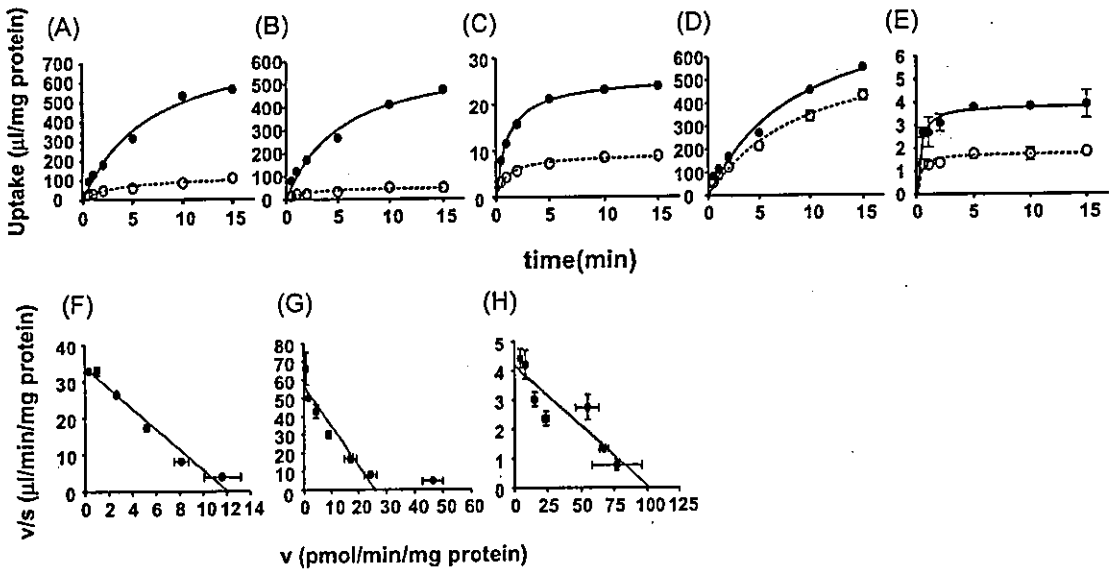

FIG. 1. Time profiles and concentration dependence of the uptake of [^{125}I]L-T4 (0.01 μM) (A and F), [^{125}I]rT_3 (0.01 μM) (B and G), [^{3}H]$E_2$17βG (1 μM) (C and H), [^{125}I]T_3 (0.01 μM) (D), and [^{3}H]E-sul (1 μM) (E) by mOatp14-HEK. The uptake by mOatp14-HEK was examined at 37 C. The *upper figures* (A–E) show the time profiles. *Closed* and *open circles* represent the uptake by mOatp14-transfected HEK293 cells and vector-control cells, respectively. The *lower figures* (F–H) show the concentration dependence as an Eadie-Hofstee plot. Specific uptake was obtained by subtracting the uptake by vector-control cells from that by mOatp14-HEK. The *solid line* represents the fitted line. Each *point* represents the mean ± SE (n = 3).

mOatp14-expressed HEK293 cells and vector-control cells. Specific uptake of [^{125}I]L-T4, [^{125}I]rT_3, and [^{3}H]$E_2$17βG by mOatp14-HEK was observed, whereas the uptake of [^{125}I]T_3 and [^{3}H]E-sul by mOatp14-HEK was slightly greater than that by vector transfected cells. The mOatp14-mediated $E_2$17βG uptake increased linearly over 2 min, whereas that of T_4 and rT_3 increased linearly over 5 min. The mOatp14-mediated uptake followed Michaelis-Menten kinetics (Fig. 1, F–H). The kinetic parameters for the uptake by mOatp14 were determined by nonlinear regression analysis and are summarized in Table 1.

The *cis*-inhibitory effect of thyroid hormones, their related compounds, and organic anions on the mOatp14-mediated uptake of [^{125}I]L-T4 was examined. D-T4, rT_3, and 3,3′,5-triiodothyroacetic acid were potent inhibitors of mOatp14, T_3, taurocholate, E-sul, $E_2$17βG, and probenecid were moderate inhibitors (Fig. 2), whereas 3,5-T2, digoxin, benzylpenicillin, and leucine (Leu) had no inhibitory effect on mOatp14-mediated transport (data not shown). The respective Ki values are summarized in Table 2.

TABLE 1. K_m, V_{max}, and V_{max}/K_m values for mOatp14-mediated transport

Substrate	K_m (μM)	V_{max} (pmol/min·mg protein)	V_{max}/K_m (μl/min·mg protein)
T_4	0.34 ± 0.03	11.7 ± 0.7	34.0 ± 3.5
rT_3	0.46 ± 0.08	25.5 ± 3.0	55.1 ± 11.4
$E_2$17βG	23.5 ± 5.2	95.8 ± 14.6	4.07 ± 1.09

The kinetic parameters for mOatp14-mediated transport were determined by nonlinear regression analysis. Results represent the mean ± SE. The data are taken from Fig. 4, A–C.

Tissue distribution of mOatp14

The tissue distribution of mOatp14 was determined by Northern blot analysis. The hybridization signal was detected predominantly in the brain at approximately 3.5 kb (Fig. 3A). The distribution of mOatp14 in the brain was examined by Western blot analysis. There were two bands nearly the expected size. The band with the greater molecular mass was detected almost ubiquitously but not in the cerebellum (Fig. 3C). Because the mRNA of mOatp14 was not detected in the cerebellum by RT-PCR (data not shown), the band detected at the lower molecular weight in the cerebellum is unlikely to be associated with mOatp14. The expression of mOatp14 in the choroid plexus-, brain homogenate-, and brain capillary-enriched fraction was examined by Western blot analysis. The enrichment factor of γGTP of the isolated brain capillary-enriched fraction was 10.7. Immunoreactive protein was detected at approximately 90,000 in the

TABLE 2. K_i values for mOatp14

Substrate	K_i (μM)	
	This study	Sugiyama *et al.* (11)
rT_3	0.91 ± 0.21	ND
D-T_4	0.27 ± 0.04	ND
T_3	24.2 ± 9.7	2.46 ± 0.96
Triac	2.15 ± 0.50	ND
$E_2$17βG	>100	ND
Probenecid	293 ± 115	39.5 ± 8.3
Estron-3-sulfate	53.1 ± 7.4	6.63 ± 1.62
Taurocholate	109 ± 32	7.24 ± 3.33

The K_i values (this study) were determined for the uptake of T_4 by mOatp14-HEK by nonlinear regression analysis. The data are taken from Fig. 6, A–H. Results represent the mean ± SE. The K_i values for the uptake of $E_2$17βG by rOatp14-HEK were cited from Sugiyama *et al.* (11). 3,5-T_2, benzylpenicillin, PAH, digoxin, Tyr, Leu, Trp, Phe had no effect. ND, Not determined.

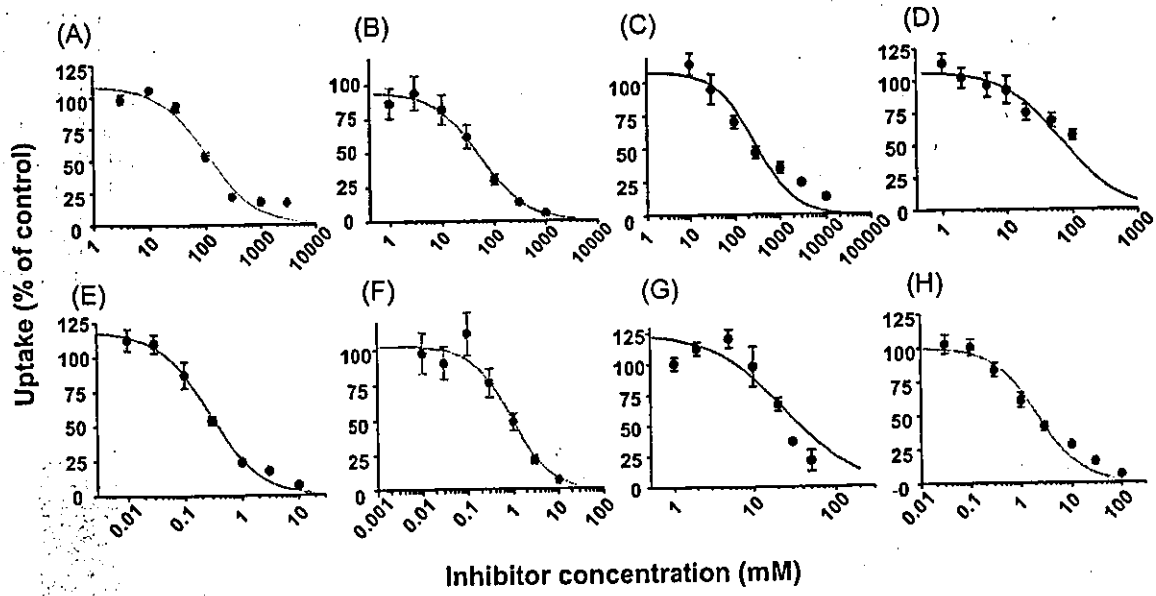

FIG. 2. Inhibition of the uptake of [^{125}I]L-T4 by mOatp14-HEK. The uptake of [^{125}I]L-T4 by mOatp14-HEK was determined in the presence and absence of inhibitors [taurocholate (A), E-sul (B), probenecid (C), $E_2$17βG (D), D-T4 (E), rT_3 (F), T_3 (G), and 3,3′,5-triiodothyroacetic acid (H)] at the concentrations indicated. The specific uptake was obtained by subtracting the uptake by vector-control cells from that by mOatp14-HEK. The *solid line* represents the fitted line obtained by nonlinear regression analysis. Each *point* represents the mean ± SE (n = 3).

choroid plexus-, brain homogenate-, and the isolated brain capillary-enriched fraction. The signal of the brain capillary band was stronger than that of the brain homogenate (Fig. 3B).

The membrane localization of mOatp14 at choroid plexus was examined by immunohistochemical staining using frozen sections of mouse brain. The signal associated with mOatp14 (*red*) was detected at the basolateral membrane of the choroid plexus epithelial cells (Fig. 3D).

In situ brain perfusion

The time profile of the uptake of [^{125}I]L-T4 by the brain (cortex and cerebellum) is shown in Fig. 4A. The uptake clearance by the cerebral cortex was 3-fold greater than that by the cerebellum (583 ± 71 *vs.* 185 ± 27 μl/min·g tissue) (Fig. 4B). The distribution volume of sucrose was 11.8 ± 0.5 and 19.2 ± 1.5 μl/g tissue for the cerebral cortex and cerebellum, respectively. The following experiments were performed for the brain uptake determined at 60 sec. The uptake by the cerebral cortex was saturable in mice (Fig. 5). The Km, Vmax, and clearance corresponding to the nonsaturable components of [^{125}I]T4 uptake by the cerebral cortex were 1.02 ± 0.16 μM, 423 ± 65 pmol/min·mg protein, and 15.6 ± 7.8 μl/min·g tissue, respectively. However, the fraction of saturation was smaller for the uptake of T_4 by the cerebellum (140 ± 30 *vs.* 44.8 ± 4.6 μl/min·g tissue at 0.01 and 10 μM, respectively). The uptake of [^{125}I]L-T4 by the cerebral cortex was inhibited markedly by taurocholate and partly by E-sul, whereas Leu, 2-aminobicyclo-(2,2,1)-heptane-2-carboxylic acid (BCH), benzylpenicillin, and digoxin had no effect. $E_2$17βG had a weak inhibitory effect (Fig. 6).

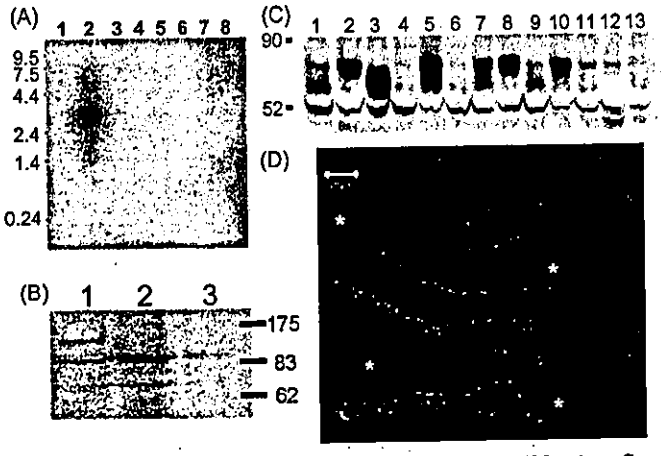

FIG. 3. Tissue distribution of mOatp14. A, Northern blotting. Commercially available mouse multiple tissue Northern blots containing 2 μg poly(A)+ RNA were hybridized for 3 h using the Oatp14 fragment as a probe. Lane 1, Heart; lane 2, brain; lane 3, spleen; lane 4, lung; lane 5, liver; lane 6, skeletal muscle; lane 7, kidney; lane 8, testis. B, Western blotting. Lane 1, Brain homogenate (30 μg); lane 2, the isolated brain capillary-enriched fraction (30 μg); lane 3, choroid plexus (two mice). These proteins were separated by SDS-PAGE (10% separating gel). Oatp14 was detected by Oatp14 polyclonal antibody. C, Western blotting. Each lane of commercially available mouse multiple brain tissue region-specific blots contained 75 μg protein. Lane 1, Frontal cortex; lane 2, posterior cortex; lane 3, cerebellum; lane 4, hippocampus; lane 5, olfactory bulb; lane 6, striatum; lane 7, thalamus; lane 8, midbrain; lane 9, entorhinal cortex; lane 10, pons; lane 11, medulla; lane 12, spinal cord; lane 13, total brain. D, Immunohistochemical staining of mOatp14. Frozen sections of mouse brain were single stained with Oatp14 polyclonal antibody (*red*). Nuclei were stained with TO-PRO-3 iodide (*blue*). *Asterisk* indicates the cerebrospinal fluid space.

Discussion

In the present study, mOatp14-mediated uptake was characterized by constructing a stable expression system, and the uptake mechanism of T_4 by the brain was investigated using the *in situ* brain perfusion technique. From the results of the uptake studies, the transport properties of mOatp14 are similar to that of rOatp14. The transport activity of T_4 and rT_3 was much greater than that of T_3, and amphipathic organic anions were accepted as substrates (Fig. 1). Furthermore, the substrate recognition by mOatp14 was investigated by a *cis*-inhibition study using thyroid hormones and related agents (Fig. 2, E–H). Because the Ki value of D-T4 (stereoisomer of L-T4) was similar to the Km value of L-T4, there is no stereosensitivity in the substrate recognition by mOatp14 (Table 2). rT_3 potently inhibited T_4 uptake, whereas T_3 had a 25-fold greater Ki value than T_4 and rT_3, and 3,5-T2 had no effect (Table 2). These results suggest the importance of iodine attached to the outer ring for high-affinity recognition of T_4 and rT_3 by mOatp14.

Probenecid, taurocholate, E-sul, and $E_2$17βG were moderate or weak inhibitors of mOatp14 (Table 2). Digoxin and benzylpenicillin, which are good substrates of Oatp2 and Oat3, respectively, had no effect on the uptake of T_4 by mOatp14, and neutral amino acids (Leu, phenylalanine, tryptophan, and tyrosine) had no effect either (data not shown). The contribution of mOatp14 and other transporters can be

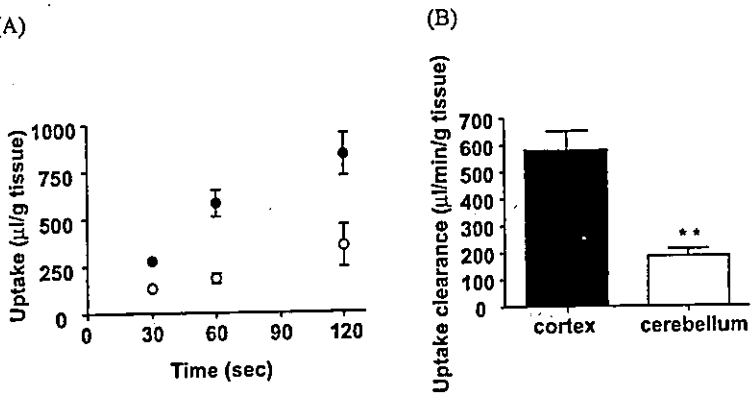

FIG. 4. A, Time profiles of the uptake of [^{125}I]L-T4 by the cerebral cortex and cerebellum. The uptake volume was determined by the *in situ* brain perfusion technique. *Closed* and *open circles* represent the uptake of [^{125}I]L-T4 by the cerebral cortex and cerebellum, respectively. Each *point* represents the mean ± SE (n = 3). B, The initial uptake clearance by the cerebral cortex and cerebellum after 60 sec. Each set of data represents the mean ± SE (n = 3). **, $P <$ 0.01.

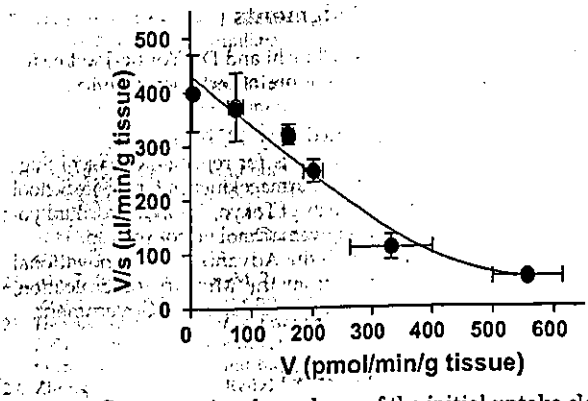

FIG. 5. Concentration dependence of the initial uptake clearance of [^{125}I]L-T4 by the cerebral cortex (concentration 0.01, 0.2, 0.5, 0.8, 10 µm). Each *point* represents the mean ± SE (n = 3). V, Uptake rate of the substrate; s, substrate concentration in the perfusate.

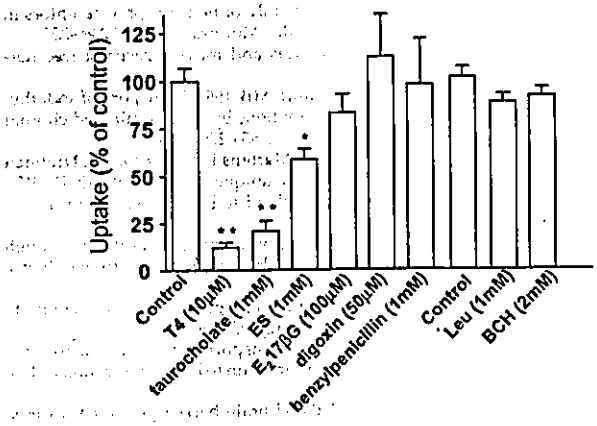

FIG. 6. Inhibition of the uptake of [^{125}I]L-T4 by the cerebral cortex. The uptake was measured in the absence (control, 100%) and presence of T_4 (10 µM), taurocholate (1 mM), E-sul (ES) (1 mM), $E_2$17βG (100 µM), digoxin (50 µM), benzylpenicillin (1 mM), Leu (1 mM), and BCH (2 mM). Each set of data represents the mean ± SE (n = 3–6). **, $P < 0.01$ and *, $P < 0.05$ relative to the corresponding control.

evaluated using these compounds as inhibitors. The Ki values of these compounds for mOatp14 were 10-fold greater than the previously reported values determined for the uptake of $E_2$17βG by rOatp14 (11). There was a discrepancy of more or less 1 order of magnitude in the Ki values of inhibitors for rat and mouse Oatp14, even though they were determined by the same methods, whereas the Km values of T_4 and $E_2$17βG for mOatp14 were comparable with those for rOatp14. Different test substrates were used to determine the Ki values of inhibitors ($E_2$17βG for rOatp14 *vs.* T_4 for mOatp14). Because $E_2$17βG had a lower inhibitory effect on T_4 uptake by mOatp14 than expected from its Km value, the Ki value of $E_2$17βG will be greater than its own Km value. As far as two substrate compounds share the same substrate recognition sites in the transporter, the Ki value of one compound for the uptake of the other should be the same as its own Km value. The discrepancies in the kinetic parameters for different substrates ($E_2$17βG and T_4) suggest that Oatp14 has at least two different substrate recognition sites. Therefore, the difference in the Ki value for the uptake of $E_2$17βG and T_4 by rat and mouse is not ascribed to the species difference but presumably accounted for by multiple recognition sites for T_4 and $E_2$17βG by mOatp14 as reported in rOatp2 (23). The Ki value of $E_2$17βG for the digoxin uptake by rOatp2 (0.04 µM) was much smaller than its Km value (1 µM) (23).

mOatp14 is widely expressed throughout the brain, and strong expression was observed in the posterior cortex, olfactory bulb, thalamus, midbrain and pons, whereas the expression in the cerebellum was below detection. Regional differences have also been observed in human OATP-F, which is not expressed in the cerebellum or pons (12). Li *et al.* (10) and Sugiyama *et al.* (11) demonstrated that rOatp14 is highly enriched in the isolated brain capillaries, and furthermore, Sugiyama *et al.* demonstrated that rOatp14 is expressed at plasma membrane of the brain capillaries in rats by immunohistochemical staining (11).

To investigate an involvement of mOatp14 in the T4 uptake across the BBB, the brain uptake of T_4 was characterized using the *in situ* brain perfusion technique. The uptake of T_4 was 3-fold greater in the cerebral cortex than in the cerebellum (Fig. 4B). A saturable component accounted for about 95% of the total uptake of T_4 by the cerebral cortex, suggesting the important role of transporters in T_4 uptake at the BBB (Fig. 5). The Km value of T_4 uptake at the cerebral cortex was almost comparable with the Km value of mOatp14 (1.02 *vs.* 0.34 µM). T_4 is highly bound to plasma T_4 binding proteins (24). Based on the free hormone hypothesis, in which free T_4 and T_3 concentrations correlate with the activity level of thyroid hormone-dependent processes (4), free T_4 will be taken up by the brain via the specific transport systems at the BBB. For mice, the range of normal serum-free T_4 is approximate 10–20 pM (25), much lower than its Km value (1.02 µM), suggesting that the transport mechanism of T_4 uptake across the BBB is not saturated under physiological conditions. In contrast, in the cerebellum, the fraction of saturation was small. These results are in good agreement with regional differences in the expression of mOatp14. Taurocholate completely inhibited the uptake of T_4 by the cerebral cortex, and E-sul and $E_2$17βG had a weak inhibitory effect. Partial inhibition by E-sul, even at a concentration sufficient to inhibit Oatp14-mediated transport completely, suggests that T_4 uptake across the BBB cannot be fully accounted for by mOatp14, and another transporter is involved in the uptake of T_4 by the cerebral cortex. The Eadie-Hofstee plot indicated that the uptake of T_4 by the brain consists of a single saturable component, suggesting that the unknown transporter has a Km value similar to T_4 with mOatp14. Because digoxin, benzylpenicillin, Leu, and BCH had no effect for the uptake of T_4 by the cerebral cortex, the involvement of Oatp2, Oat3, and large neutral amino acid transporters can be excluded. However, several transporters are identified as thyroid hormone transporters up to now (26, 27), and this time we could not estimate the contribution of some transporters. Further studies are necessary to identify the taurocholate-inhibitable transporter involved in the uptake of T_4 together with mOatp14.

In addition to the brain capillaries, Western blot analysis detected mOatp14 protein in the choroid plexus in which it is located on the basolateral membrane (Fig. 3, B and D). Previously, *in situ* choroid plexus perfusion experiments in

sheep revealed that a saturable mechanism is responsible for the uptake of T_4 through the choroid plexus from blood side to the cerebrospinal fluid (28). Apparent Km value with respect to the concentration in the injectate was 11 μM. However, taking into consideration the dilution factor after the injection, the corrected Km value was to be 1.6 μM, comparable with that determined in this study for the uptake by the cerebral cortex across the BBB. mOatp14 may play a role in the uptake of T_4 at the basolateral side of the choroid plexus epithelial cells.

The present study highlights the importance of membrane transporters, especially Oatp14, for the brain uptake of T_4 across the BBB. In addition to the BBB and blood-cerebrospinal fluid barrier, transporters will play an important role in the disposition of thyroid hormones in the central nervous system. Carrier-mediated uptake of T_4 and T_3 has been reported in primary cultured neuronal cells (29). Although the transporter uptake by brain parenchymal cells has not been identified, there are some likely candidate transporters. OATP-E, another Oatp/OATP isoform, is known to accept thyroid hormones as substrates (30) and is expressed in the brain (30). In addition to Oatp/OATP isoforms, MCT8 has been identified as a thyroid hormone transporter (17). MCT8 is expressed weakly in the brain but most abundantly in the liver (17). Recently Dumitrescu *et al.* (31) reported that mutations in the MCT8 gene are associated with thyroid hormonal and neurological abnormalities in humans, although whether these are due to the functional loss of MCT8 in the central nervous system remains to be elucidated. Further studies are necessary to determine the roles of transporters in regulating the disposition of thyroid hormones in the central nervous system.

Thyroid hormones are activated/inactivated by deiodinases in the brain. Of three subtypes, types 2 and 3 deiodinases are expressed in the brain. Type 2 deiodinase is responsible for the conversion T_4 to T_3, whereas type 3 deiodinase inactivates thyroid hormone by converting T_4 to rT_3, and T_3 to T_2 (32, 33). In the brain, type 2 deiodinase has been shown to be predominantly expressed in the nonneuronal cells and glial cells, such as tanycytes and astrocytes (32), whereas type 3 deiodinase is expressed in the neurons (33). Therefore, it can be hypothesized that T_4 is transported into the brain via the BBB by specific transport systems followed by activation to T_3 mainly in nonneuronal and glial cells. Thereafter, T_3, produced by nonneuronal and glial cells, is taken up by neuronal cells to exert its action via the nuclear receptors followed by inactivation by type 3 deiodinase. Membrane transport processes in nonneuronal and glial cells and neurons will play an important role in regulating the effect of thyroid hormones in the central nervous system together with deiodinases.

In conclusion, taurocholate-sensitive transporters play a predominant role in the uptake of T_4 across the BBB. It is suggested that mOatp14 accounts for E-sul inhibitable fraction, at least partly, and the E-sul-insensitive fraction is accounted for by unknown transporters. In addition to the BBB, Oatp14 may also play a role in the uptake of T_4 in the choroid plexus.

Acknowledgments

We are grateful to Dr. Toshimasa Ohnishi and Dr. Young-Joo Lee for their kind instruction to perform *in situ* brain perfusion in mice.

Received January 19, 2004. Accepted May 19, 2004.

Address all correspondence and requests for reprints to: Yuichi Sugiyama, Ph.D., Department of Molecular Pharmacokinetics, Graduate School of Pharmaceutical Sciences, The University of Tokyo, 7-3-1 Hongo, Bunkyo-ku, Tokyo 113-0033, Japan. E-mail: sugiyama@mol.f.u-tokyo.ac.jp.

This study was performed through the Advanced and Innovational Research program in Life Sciences from the Ministry of Education, Culture, Sports, Science and Technology, the Japanese Government.

References

1. **Bernal J** 2002 Action of thyroid hormone in brain. J Endocrinol Invest 25: 268–288
2. **Sarkar PK** 2002 In quest of thyroid hormone function in mature mammalian brain. Indian J Exp Biol 40:865–873
3. **Alvarez-Dolado M, Iglesias T, Rodriguez-Pena A, Bernal J, Munoz A** 1994 Expression of neurotrophins and the trk family of neurotrophin receptors in normal and hypothyroid rat brain. Brain Res Mol Brain Res 27:249–257
4. **Ekins R** 1992 The free hormone hypothesis and measurement of free hormones. Clin Chem 38:1289–1293
5. **Dratman MB, Crutchfield FL, Schoenhoff MB** 1991 Transport of iodothyronines from bloodstream to brain: contributions by blood:brain and choroid plexus:cerebrospinal fluid barriers. Brain Res 554:229–236
6. **Cheng LY, Outterbridge LV, Covatta ND, Martens DA, Gordon JT, Dratman MB** 1994 Film autoradiography identifies unique features of [125I]3,3'5'-(reverse) triiodothyronine transport from blood to brain. J Neurophysiol 72: 380–391
7. **Pardridge WM** 1979 Carrier-mediated transport of thyroid hormones through the rat blood-brain barrier: primary role of albumin-bound hormone. Endocrinology 105:605–612
8. **Hagen GA, Solberg Jr LA** 1974 Brain and cerebrospinal fluid permeability to intravenous thyroid hormones. Endocrinology 95:1398–1410
9. **Banks WA, Kastin AJ, Michals EA** 1985 Transport of thyroxine across the blood-brain barrier is directed primarily from brain to blood in the mouse. Life Sci 37:2407–2414
10. **Li JY, Boado RJ, Pardridge WM** 2001 Blood-brain barrier genomics. J Cereb Blood Flow Metab 21:61–68
11. **Sugiyama D, Kusuhara H, Taniguchi H, Ishikawa S, Nozaki Y, Aburatani H, Sugiyama Y** 2003 Functional characterization of rat brain-specific organic anion transporter (Oatp14) at the blood-brain barrier: high affinity transporter for thyroxine. J Biol Chem 278:43489–43495
12. **Pizzagalli F, Hagenbuch B, Stieger B, Klenk U, Folkers G, Meier PJ** 2002 Identification of a novel human organic anion transporting polypeptide as a high affinity thyroxine transporter. Mol Endocrinol 16:2283–2296
13. **Abe T, Kakyo M, Sakagami H, Tokui T, Nishio T, Tanemoto M, Nomura H, Hebert SC, Matsuno S, Kondo H, Yawo H** 1998 Molecular characterization and tissue distribution of a new organic anion transporter subtype (oatp3) that transports thyroid hormones and taurocholate and comparison with oatp2. J Biol Chem 273:22395–22401
14. **Reichel C, Gao B, Van Montfoort J, Cattori V, Rahner C, Hagenbuch B, Stieger B, Kamisako T, Meier PJ** 1999 Localization and function of the organic anion-transporting polypeptide Oatp2 in rat liver. Gastroenterology 117:688–695
15. **Friesema EC, Docter R, Moerings EP, Verrey F, Krenning EP, Hennemann G, Visser TJ** 2001 Thyroid hormone transport by the heterodimeric human system L amino acid transporter. Endocrinology 142:4339–4348
16. **Matsuo H, Tsukada S, Nakata T, Chairoungdua A, Kim DK, Cha SH, Inatomi J, Yorifuji H, Fukuda J, Endou H, Kanai Y** 2000 Expression of a system L neutral amino acid transporter at the blood-brain barrier. Neuroreport 11: 3507–3511
17. **Friesema EC, Ganguly S, Abdalla A, Manning Fox JE, Halestrap AP, Visser TJ** 2003 Identification of monocarboxylate transporter 8 as a specific thyroid hormone transporter. J Biol Chem 278:40128–40135
18. **Hearn MT, Hancock WS, Bishop CA** 1978 High-pressure liquid chromatography of amino acids, peptides and proteins. V. Separation of thyroidal iodoamino acids by hydrophilic ion-paired reversed-phase high-performance liquid chromatography. J Chromatogr 157:337–344
19. **Dagenais C, Rousselle C, Pollack GM, Scherrmann JM** 2000 Development of an *in situ* mouse brain perfusion model and its application to mdr1a P-glycoprotein-deficient mice. J Cereb Blood Flow Metab 20:381–386
20. **Yamaoka K, Tanigawara Y, Nakagawa T, Uno T** 1981 A pharmacokinetic analysis program (multi) for microcomputer. J Pharmacobiodyn 4:879–885
21. **Ball HJ, McParland B, Driussi C, Hunt NH** 2002 Isolating vessels from the mouse brain for gene expression analysis using laser capture microdissection. Brain Res Brain Res Protoc 9:206–213

22. Dallaire L, Tremblay L, Beliveau R 1991 Purification and characterization of metabolically active capillaries of the blood-brain barrier. Biochem J 276(Pt 3):745–752
23. Sugiyama D, Kusuhara H, Shitara Y, Abe T, Sugiyama Y 2002 Effect of 17 β-estradiol-D-17 β-glucuronide on the rat organic anion transporting polypeptide 2-mediated transport differs depending on substrates. Drug Metab Dispos 30:220–223
24. Hulbert AJ 2000 Thyroid hormones and their effects: a new perspective. Biol Rev Camb Philos Soc 75:519–631
25. Palha JA, Episkopou V, Maeda S, Shimada K, Gottesman ME, Saraiva MJ 1994 Thyroid hormone metabolism in a transthyretin-null mouse strain. J Biol Chem 269:33135–33139
26. Abe T, Suzuki T, Unno M, Tokui T, Ito S 2002 Thyroid hormone transporters: recent advances. Trends Endocrinol Metab 13:215–220
27. Hennemann G, Docter R, Friesema EC, de Jong M, Krenning EP, Visser TJ 2001 Plasma membrane transport of thyroid hormones and its role in thyroid hormone metabolism and bioavailability. Endocr Rev 22:451–476
28. Zheng W, Deane R, Redzic Z, Preston JE, Segal MB 2003 Transport of L-[125I]thyroxine by *in situ* perfused ovine choroid plexus: inhibition by lead exposure. J Toxicol Environ Health A 66:435–451
29. Chantoux F, Blondeau JP, Francon J 1995 Characterization of the thyroid hormone transport system of cerebrocortical rat neurons in primary culture. J Neurochem 65:2549–2554
30. Fujiwara K, Adachi H, Nishio T, Unno M, Tokui T, Okabe M, Onogawa T, Suzuki T, Asano N, Tanemoto M, Seki M, Shiiba K, Suzuki M, Kondo Y, Nunoki K, Shimosegawa T, Iinuma K, Ito S, Matsuno S, Abe T 2001 Identification of thyroid hormone transporters in humans: different molecules are involved in a tissue-specific manner. Endocrinology 142:2005–2012
31. Dumitrescu AM, Liao XH, Best TB, Brockmann K, Refetoff S 2004 A novel syndrome combining thyroid and neurological abnormalities is associated with mutations in a monocarboxylate transporter gene. Am J Hum Genet 74:168–175
32. Guadano-Ferraz A, Obregon MJ, St. Germain DL, Bernal J 1997 The type 2 iodothyronine deiodinase is expressed primarily in glial cells in the neonatal rat brain. Proc Natl Acad Sci USA 94:10391–10396
33. Tu HM, Legradi G, Bartha T, Salvatore D, Lechan RM, Larsen PR 1999 Regional expression of the type 3 iodothyronine deiodinase messenger ribonucleic acid in the rat central nervous system and its regulation by thyroid hormone. Endocrinology 140:784–790

Endocrinology is published monthly by The Endocrine Society (http://www.endo-society.org), the foremost professional society serving the endocrine community.

Available online at www.sciencedirect.com

SCIENCE DIRECT

ELSEVIER

Advanced Drug Delivery Reviews 56 (2004) 1741–1763

Advanced DRUG DELIVERY Reviews

www.elsevier.com/locate/addr

Efflux transport systems for organic anions and cations at the blood–CSF barrier

Hiroyuki Kusuhara, Yuichi Sugiyama*

Graduate School of Pharmaceutical Sciences, University of Tokyo, 7-3-1 Hongo, Bunkyo-ku, Tokyo 113-0033, Japan

Received 10 August 2003; accepted 4 July 2004
Available online 25 August 2004

Abstract

The choroid plexus (CP), located in the lateral, third and fourth ventricles, is the site of elimination of xenobiotics and endogenous waste from the cerebrospinal fluid (CSF) together with convective flow associated with CSF turnover. Active efflux transport systems, as well as metabolic enzymes in the choroid plexus epithelial cells (CPE), which form a tight monolayer, play a protective role by facilitating the elimination of xenobiotics including drugs and endogenous waste from the CSF to prevent their accumulation in the central nervous system. Except in the case of lipophilic cationic and neutral compounds, uptake and efflux transporters carry out the vectorial transport across the cell monolayer to transfer their common substrates efficiently from the CSF to the blood side. Many published studies have given us some insights into the uptake mechanisms for organic compounds at the brush border side of the CP. Organic anion transporters, such as Oatp3 and Oat3, play a major role in the uptake of amphipathic and hydrophilic organic anions, respectively, at the brush border surface of the CPE, while the organic cation transporters, Oct2 and/or Oct3, have been suggested to be involved in the uptake of hydrophilic organic cations. In contrast, the molecular characteristics of basolateral transporters have not been fully elucidated. Mrp1 is involved in the excretion of etoposide at the basolateral membrane of the CPE, but its contribution to the excretion of organic anions, especially amphipathic conjugated metabolites, remains controversial. The present manuscript summarizes the efflux transport mechanisms at the choroid plexus and focuses on the molecular characteristics of these transporters.

Keywords: Efflux transport; Organic anion; Organic cation; OCT; OAT; OATP; MRP

Abbreviations: ABC, ATP-binding cassette; BBB, blood–brain barrier; BCSFB, blood–cerebrospinal fluid barrier; BLM, basolateral membrane; BBM, brush border membrane; CP, choroid plexus; CPE, choroid plexus epithelial cells; OAT, organic anion transporter; OCT, organic cation transporter; OATP, organic anion-transporting polypeptide; PEPT, peptide transporter; MRP, multidrug resistance-associated protein; P-gp, P-glycoprotein; i.c.v., intracerebroventricular; E217βG, 17β-estradiol-D-17β glucuronide; FCCP, carbonyl-cyanide *p*-trifluoromethoxyphenylhydrazone; NMN, *N*-methylnicotineamide; PAH, *p*-aminohippurate; PGE2, prostaglandin E2; TEA, tetraethylammonium.

* Corresponding author. Tel.: +81 3 5841 4774; fax: +81 3 5841 4766.
E-mail address: sugiyama@mol.f.u-tokyo.ac.jp (Y. Sugiyama).

0169-409X/$ - see front matter © 2004 Published by Elsevier B.V.
doi:10.1016/j.addr.2004.07.007

Contents

1. Introduction . . . 1742
2. Pharmacokinetic quantification of efflux transport from the CSF . . . 1744
3. Molecular characteristics of drug transporters . . . 1744
3.1. Organic anion-transporting polypeptide (Oatp/OATP; SLCO) . . . 1744
3.2. Organic ion transporter (SLC22A) . . . 1746
3.2.1. Organic anion transporter (Oat/OAT; SLC22A) . . . 1746
3.2.2. Organic cation transporter (Oct/OCT; SLC22A) . . . 1747
3.2.3. OCTN (SLC22A) . . . 1748
3.3. Peptide transporter (PEPT; SLC15A) . . . 1748
3.4. ABC transporters . . . 1748
3.4.1. Multidrug resistance-associated protein (MRP; ABCC) . . . 1748
3.4.2. P-glycoprotein (ABCB1) . . . 1749
4. Efflux transport mechanisms for organic anions in the choroid plexus . . . 1749
4.1. Amphipathic organic anions . . . 1749
4.2. Hydrophilic organic anions . . . 1752
5. Efflux transport mechanism for organic cations in the choroid plexus . . . 1754
5.1. Cimetidine . . . 1755
5.2. Tetraethylammonium and choline . . . 1755
6. Discussion and future aspects . . . 1757
References . . . 1757

1. Introduction

The choroid plexus (CP) is a leaf-like, highly vascularized organ that protrudes into the ventricles. It secretes the cerebrospinal fluid (CSF) which fills the ventricular system and the subarachnoideal space, and circulates around the brain and spinal cord before it is reabsorbed into the blood circulation primarily by the arachnoid villi [1,2]. The CSF maintains the working environment of the brain by providing buoyancy to protect the brain and by acting as a buffer reservoir or as a source of necessary osmolytes. The CP consists of fenestrated capillaries surrounded by a tight monolayer of epithelial cells. The choroid plexus epithelial cells (CPE) are polarized to form brush border (BBM) and basolateral (BLM) membranes facing towards the CSF and plasma, respectively. Due to fenestrated capillaries in the CP, compounds in the blood have free access to the BLM of the CPE; however, tightly sealed cell junctions between the epithelial cells prevent free exchange of compounds between the blood and CSF, and provide a barrier function between the CSF and the blood circulation (blood–CSF barrier). In addition, the CPE has detoxification systems, including metabolic enzymes and efflux transport systems, to facilitate the elimination of xenobiotics and endogenous wastes from the CSF to the circulating blood. This, together with the blood–brain brain barrier formed by brain capillary endothelial cells, prevents their accumulation in the central nervous system [3–8]. Drugs acting in the central nervous system have to overcome these

Notes to Table 1:
Tissue distribution: k, kidney; li, liver; lu, lung; b, brain; si, small intestine; t, testis; r, retina; pl, placenta; m, muscle; bl, bladder; e, eye; cp, choroid plexus; h, heart; sp, spleen; tg, thyroid gland; ag, adrenal gland; bc, brain capillary; Membrane localization: AM, abluminal membrane; LM, luminal membrane; SM, sinusoidal membrane; CM, canalicular membrane; BLM, basolateral membrane; BBM, brush border membrane; OA, organic anion.

[a] Controversial.

[b] Localization of the chimeric protein (rOct2-GFP).

Table 1
Drug transporters potentially involved in the efflux transport across the CP

Name	Species	Locus ID	Gene symbol	Tissue distribution	Membrane localization	Transport mechanism
Facilitate, secondary/tertiary active transporter organic anion-transporting polypeptide (Oatp/OATP) family						
Oatp2	rat	170698	*Slco1a4*/Oatp1a4	li, b, r, cp	SM(li), LM/AM(bc), BLM(cp)	ND
Oatp3	rat	80900	*Slco1a5*/Oatp1a5	k, r, b, lu, si, cp[a]	BBM	ND
OATP A	human	6579	*SLCO1A2*/OATP1A2	b, low: k, li, lu, t	LM/AM(bc)	ND
Oatp9/moat1	rat	140860	*Slco2b1*/Oatp2b1	ubiquitously		ND
OATP B	human	11309	*SLCO2B1*/OATP2B1	ubiquitously	SM(li), BBM(si)	ND
Oatp12	rat	171144	*Slco4a1*/Oatp4a1	ubiquitously	ND	ND
OATP E	human	28231	*SLO4A1*/OATP4A1	ubiquitously	ND	ND
Oatp14/BSAT1	rat	84511	*Slco1c1*/Oatp1c1	b, cp	LM/AM(bc)	ND
OATP-F	human	53919	*SLCO1C1*/OATP1C1	b, t	ND	ND
Organic anion transporter (Oat/OAT) family						
Oat1	rat	29509	*Slc22a6*	k, cp	BLM(k)	OA/dicarboxylate antiport
OAT1	human	9356	*SLC22A6*	k	BLM	ND
Oat2/NLT	rat	89776	*Slc22a7*	li, k (female), cp	SM(li), BBM(k)	ND
OAT2	human	10864	*SLC22A7*	li, k	BLM(k)	ND
Oat3/Roct	mouse	19879	*Slc22a8*	k	ND	ND
Oat3	rat	83500	*Slc22a8*	li(male), k, b, e, cp	BLM(k), AM(bc), BBM(cp)	OA/dicarboxylate antiport
OAT3	human	9376	*SLC22A8*	k	BLM	OA/dicarboxylate antiport
Organic cation transporter (Oct/OCT) family						
Oct2	rat	19503	*Slc22a2*	k, b, cp	BLM(k), BBM(cp)[b]	facilitative
OCT2	human	6582	*SLC22A2*	k (distal tubul)	BLM	facilitative
Oct3	rat	29504	*Slc22a3*	ubiquitously	ND	facilitative
OCT3	human	6581	*SLC22A3*	ubiquitously	ND	facilitative
Octn/OCTN family						
Octn1	rat	19503	*Slc22a2*	li, si, b, k, h, pl	ND	
OCTN1	human	6582	*SLC22A2*	ubiquitously	ND	H^+ antiport
Octn2/CT1	rat	29504	*Slc22a3*	ubiquitously	ND	
OCTN2	human	6581	*SLC22A3*	ubiquitously	ND	Na^+ symport
Peptide transporter						
PEPT2	rat	60577	*Slc15a2*	k, b, lu, sp	BBM	H^+ symport
PEPT2	human	6565	*SLC15A2*	k	ND	H^+ symport
ABC transporter P-glycoprotein						
Mdr1a	mouse	18671	*Abcb1a*	si, h, b, li, k, lu, t	CM(li), BBM(si, k), LM(bc)	primary active
Mdr1b	mouse	18669	*Abcb1b*	pl (during pregnancy), ag, k, h	CM(li), BBM(k)	primary active
MDR1	human	5243	*ABCB1*	b, li, k, si	CM(li), BBM(si), LM(bc)	primary active
Multidrug resistance-associated protein (Mrp/MRP) family						
Mrp1	mouse	17250	*Abcc1*			primary active
Mrp1	rat	24565	*Abcc1*	b, cp	BLM(cp)	primary active
MRP1	human	4363	*ABCC1*	lu, sp, tg, t, bl, ag	ND	primary active
Mrp4	mouse	239273	*Abcc4*	ND	ND	primary active
MRP4	human	10257	*ABCC4*	ubiquitously	BBM(k)	primary active
Mrp5	mouse	27416	*Abcc5*	ND	ND	primary active
MRP5	human	10057	*ABCC5*	ubiquitously	ND	primary active

barriers to achieve clinically significant concentrations in the central nervous system.

The efflux transport of organic compounds across the cell monolayer is characterized by vectorial transport, which plays a major role in the hepatobiliary transport and urinary secretion of organic anions and hydrophilic organic cations. Recently, a number of transporters have been cloned and their functional characterization has been carried out [6,9–15]. This has allowed the elucidation of the molecular characteristics of the efflux transport systems expressed at the CP as summarized in Table 1. The primary purpose of the present manuscript is to illustrate the efflux transport systems for organic anions and cations in the CP.

2. Pharmacokinetic quantification of efflux transport from the CSF

A sequential determination of the CSF concentration after intracerebroventricular (i.c.v.) administration (C_{CSF}) allows us to determine the elimination rate constant (k_e) as described by the following differential equation,

$$\frac{dC_{CSF}}{dt} = -k_e C_{CSF} = -CL_{CSF}/V_{d,CSF} C_{CSF} \quad (1)$$

where CL_{CSF} represents the elimination clearance from the CSF. The time profile of the drug concentration in the CSF is affected not only by the elimination clearance, but also by the distribution volume in the ventricles ($V_{d,CSF}$). The CL_{CSF} is experimentally obtained from the elimination rate constant (k_e) and distribution volume ($V_{d,CSF}$). $V_{d,CSF}$ can be calculated using the amount of drug injected into the ventricles and the initial CSF concentration extrapolated to time 0 assuming rapid equilibrium of distribution in the ventricles.

The CL_{CSF} represents the sum of the elimination clearance of three different elimination routes from the CSF, i.e. (1) bulk flow rate, (2) active efflux through the CP and (3) diffusion into the brain parenchyma through the ependyma surface followed by efflux across the brain capillaries and/or metabolism. Suzuki et al. [17] introduced a spatially distributed model, which was initially developed by Collins and Dedrick [16], to handle each elimination process quantitatively. Based on this model, the CL_{CSF} can be expressed by the following equation,

$$CL_{CSF} = Q_{CSF} + \sqrt{A_r^2 D_1 PS_{eff} V_{br}} + PS_{eff,cp} \quad (2)$$

where Q_{CSF} is the bulk flow rate, A_r is the ependymal surface area, D_1 is the apparent diffusion constant for the ligand in the brain extracellular fluid, V_{br} is the volume of distribution in the brain, defined as the brain concentration divided by the concentration in the brain extracellular fluid, and PS_{eff} and $PS_{eff,CP}$ are the PS products for the efflux of ligand across the brain capillaries and CP, respectively. The second and third terms represent the elimination via the brain parenchyma and the CP, respectively. The efflux clearance across the brain capillaries (PS_{eff}) can be evaluated in separate experiments, such as in vivo microdialysis and the brain efflux index method [18,19]. The details of these experimental methods are given in Ref. [19]. Ogawa et al. [20] applied this model to analyze the elimination of a β-lactam antibiotic, benzylpenicillin, from the CSF. According to this analysis, the efflux transport through the CP accounted for the major part of the total elimination clearance (64%), while the remainder is accounted for by the CSF convective flow (12%) and elimination via the brain parenchyma followed by the efflux across the brain capillaries (24%).

3. Molecular characteristics of drug transporters

In this section, the molecular characteristics of the uptake transporters, such as Oatp/OATP, Oat/OAT, Oct/OCT and PEPT are described, as well as the ABC transporters, such as Mrp/MRP and P-glycoprotein. The prefixes m, r and h represent different species, i.e. mice, rats and humans, in the following text.

3.1. Organic anion-transporting polypeptide (Oatp/OATP; SLCO)

The organic anion-transporting polypeptides (referred to as Oatp in rodents and OATP in humans) belong to the growing gene family of organic anion/prostaglandin transporters that mediate sodium-independent transport of numerous endogenous and xenobiotic amphipathic compounds. They are classified

within the gene superfamily of solute carriers (SLC) as the *SLCO* gene family (Human Gene Nomenclature Committee DataBase). Fourteen members of the *Oatp/OATP* family have been identified in rodents and humans [12]. Review articles of the Oatp/OATP family are available in Refs. [12,21,22].

In the CP, rOatp1 (*Slco1a1*, Oatp1a1) was initially identified along the brush border membrane (BBM) of the CPE [23]. However, recent publications have revealed that rOatp3 (*Slco1a5*, Oatp1a5), and not rOatp1, is the most abundant isoform in the CP [24–26] where it is localized to the BBM [25]. Due to the high degree of homology between rOatp1 and rOatp3, this discrepancy is presumably due to the cross-reaction of probes. Among rat isoforms, rOatp2 (*Slco1a4*, Oatp1a4) has been identified at the BLM of the CPE [27]. In addition, the expression of rOatp9 (*Slco2b1*, Oatp2b1), rOatp12 (*Slco4a1*, Oatp4a1) and rOatp14 (*Slco1c1*, Oatp1c1) has been reported, but the expression of Oatp4 (*Slco1b2*, Oatp1b2), Oatp5 (*Slco1a6*, Oatp1a6) and Oat-K1/Oat-K2 (*Slco1a3*, Oatp1a3) was below the detection limit [26,28]. According to the quantification by Choudhuri [26], the mRNA expression of rOatp9, rOatp12 and rOatp2 in the rat CP is much lower than that of rOatp3.

rOatp3 was isolated from the rat retina cDNA library using homology cloning [29]. The cDNA encodes a 670-amino-acid protein of approximately 80 kDa with 12 putative transmembrane domains. The tissue distribution of rOatp3 is still under discussion. Northern blot analysis using the 3′ non-coding region as a probe revealed its expression in the kidney [29]. However, subsequent analyses using the RNase protection assay revealed its expression in the brain, small intestine, lung and retina [30], but not in the kidney and liver. Li et al. [31] quantified the Oatp3 mRNA expression using the branched DNA signal amplification method. An abundant Oatp3 expression was found in the lung, cerebellum and female cerebral cortex and, to a lesser extent, in the intestine. Functional expression studies of rOatp3 revealed its broad substrate specificity including amphipathic organic anions, such as bile acids, E217βG, estrone sulfate, dehydroepiandrosterone sulfate, and thyroid hormones [24,25,29,32]. In *Xenopus laevis* oocytes, the K_m values of estrone sulfate, dehydroepiandrosterone sulfate and estrone sulfate for rOatp3 were greater than those for rOatp1 and rOatp2 [32], whereas they were similar to those for rOatp1 when they are expressed in LLC-PK1 cells [25].

rOatp2 was isolated from the rat brain and retina cDNA library using homology cloning [29,33]. The cDNA encodes a 661-amino-acid protein with an apparent molecular mass of 92 kDa [34]. Its substrate specificity is similar to rOatp1 and rOatp3 [32], but cardiac glycosides, such as ouabain and digoxin, show a higher affinity for rOatp2 [32,33]. In addition, rOatp2 accepts bulky organic cations, such as *N*-(4,4-azo-n-pentyl)-21-deoxyajmalinium, *N*-methyl-quinidine, *N*-methyl-quinine and rocuronium, as well as anionic peptides, such as BQ-123, [D-Pen2,D-Pen5]enkephalin and deltorphin II [35,36]. Bi-directional transport by rOatp2 has been shown by Li et al. [37]. They demonstrated that taurocholate uptake by rOatp2-expressed oocytes was increased in the presence of an outward concentration gradient of taurocholate and glutathione conjugates. Thus, rOatp2 at the BLM of the CP may be involved in the excretion of organic anions, as well as uptake from the circulating blood.

OATP-A (*SLCO1A2*, OATP1A2) is the human isoform which exhibits the highest homology with rOatp2 and rOatp3 [12,38]. Its cDNA is abundantly expressed in the brain and, to a lesser extent, in the lung, liver, kidney and testis [39,40]. It is ubiquitously distributed in the brain, although its expression in the CP remains unknown [41]. Functional expression studies of OATP-A show its broad substrate specificity, including ouabain (cardiac glycoside), type II organic cations, such as *N*-(4,4-azo-n-pentyl)-21-ajmalinium, *N*-methylquinine and *N*-methylquinidine, as well as amphipathic organic anions [35,38,40].

rOatp9 is a rodent ortholog of hOATP-B (*SLCO2B1*, OATP2B1). rOatp9 and hOATP-B are ubiquitously expressed in the body [42–44]. Northern blot and in situ hybridization analyses of rat brain further indicated that Oatp9 mRNA is widely distributed in the neuronal cells of the central nervous system, especially in the hippocampus and cerebellum, but the expression in the CP was below the detection limit in this analysis [42]. hOATP-B has been shown to be localized to the sinusoidal membrane in the liver and the BBM of intestinal epithelial cells [44,45]. The substrates of rOatp9 include

prostaglandins (PGE_2, PGD_2 and PGE_1), leukotriene C_4 and thromboxan B_2, while the substrates of hOATP-B include bromosulfophtalein, estrone sulfate, dehydroepiandrosterone sulfate and pravastatin [43–45].

rOatp12 is a rodent ortholog of hOATP-E (*SLCO4A1*, OATP4A1). The tissue distribution of hOATP-E is ubiquitous [46]. Triiodothyronine (T3) is the only substrate of rOatp12 which has been reported [46], while the substrates of hOATP-E include T3, thyroxine (T4), reverse T3 and E217βG [43,46].

rOatp14 was originally referred to as BBB-specific anion transporter 1 (BSAT1), which was isolated using gene microarray techniques by comparing the gene-expression profile of cDNA from the brain capillaries with that from the liver and kidney [47]. rOatp14 cDNA consists of 2148 base pairs that encode a 716-amino-acid residue protein with 12 putative membrane-spanning domains. The substrates of rOatp14 include organic anions, such as E217βG, cerivastatin and troglitazone sulfate, as well as T4 and reverse T3 [28]. T4 shows the highest transport activity and affinity for rOatp14 among the known substrates [28]. Western blot analysis detected a band in the CP in addition to the brain capillary enriched fraction [28]. OATP-F (*SLCO1C1*, OATP1C1), the human ortholog of rOatp14, accepts T4 and reverse T3 specifically as substrates, and the transport activity of organic anions by OATP-F is low [48].

3.2. Organic ion transporter (SLC22A)

The organic ion transporter family is a superfamily which consists of Oat/OAT, Oct/OCT, Octn/OCTN, CT2 and URAT1. CT2 and URAT1 are transporters for carnitine and urate, respectively [49,50]. This section focuses on the molecular characteristics of Oat/OAT, Oct/OCT and Octn/OCTN.

3.2.1. Organic anion transporter (Oat/OAT; SLC22A)

Four *OAT* genes (OAT1–OAT4 in human, and Oat1–Oat3 and Oat5 in rodents) have been identified. Review articles of the Oat/OAT family are available in Refs. [9,11,13,14,51–53]. RT-PCR analysis revealed the expression of three rat Oat mRNAs in the CP [54] and quantification by Choudhuri et al. [26] revealed that rOat3 (*Slc22a8*) is the most abundant isoform expressed in the CP followed by rOat1 (*Slc22a6*) and rOat2 (*Slc22a7*). Western blot analysis revealed the protein expression of rOat3 in the CP, but no rOat1 protein was detected in the CP [55]. In human CP, immunohistochemical staining showed both hOAT1 (*SLC22A6*) and hOAT3 (*SLC22A8*) are expressed although their membrane localization remains to be elucidated [56].

The partial sequence of rOat3 was cloned from rat brain cDNA using degenerative primers designed for the conserved region among rOat1, rOat2 and rOct1. Its full-length cDNA was cloned from rat kidney cDNA library using the partial sequence as a probe [57]. The cDNA encodes 551 amino acids with 12 putative transmembrane domains. Northern blot analysis revealed its abundant expression in the liver, kidney, and, to lesser extent, in the brain and eye [57], whereas hOAT3 is predominantly expressed in the kidney [58]. Immunofluorescence studies show that the membrane localization of rOat3 is the BBM of the CP and the BLM of the renal proximal tubules [55,59]. Functional expression in *X. laevis* oocytes and mammalian cells has revealed that rOat3 has a broad substrate specificity including amphipathic organic anions, such as E217βG, estrone sulfate and dehydroepiandrosterone sulfate; hydrophilic organic anions, such as PAH and benzylpenicillin; and the organic cation, cimetidine [55,57,59–63].

Estrone sulfate uptake and efflux via rOAT3 are not *trans*-stimulated by ochratoxin A, PAH or estrone sulfate in rOat3-cRNA injected *Xenopus* oocytes[57]. In contrast, Sweet et al. [64] demonstrated that estrone sulfate and PAH uptake by rOat3-expressing oocytes was stimulated by an outward concentration gradient of glutarate formed by co-expression of the sodium-dicarboxylate cotransporter (NaDC-1) in *X. laevis* oocytes. The efflux of glutarate from inside the cells was greater in hOAT3-expressing oocytes than in control oocytes and was stimulated by extracellular OAT3 substrates, such as α-ketoglutarate, glutarate, PAH, cimetidine and urate. Estrone sulfate inhibited the efflux [65]. Thus, it is likely that rOat3/hOAT3 is an exchanger and an outward concentration gradient of dicarboxylates, such as α-ketoglutarate, formed by the sodium-dependent dicarboxylate co-transporter and the TCA cycle, may drive rOat3-mediated transport.

The Oat3 knockout mouse was established by Sweet et al. [54] and this gives more direct insight

into its role in the kidney and CP. This mouse strain is healthy and exhibits no significant physiological abnormalities compared with the corresponding wild-type mouse. Most of the uptake of amphipathic organic anions, such as taurocholate and estrone sulfate, is markedly reduced in kidney slices from the mOat3 knockout mouse compared with that from the wild-type mouse [54]. In addition, the accumulation of fluorescein is markedly reduced in the isolated CP from the mOat3 knockout mouse [54].

rOat1 has been isolated as a "classical" organic anion transporter at the BLM of the renal proximal tubules by expression cloning using *X. laevis* oocytes and it accepts PAH as a typical substrate [66,67]. rOat1 is predominantly expressed in the kidney and shows broad substrate specificity to organic anions, such as PAH, β-lactam antibiotics, nucleoside analogs and nonsteroidal anti-inflammatory drugs [11,13,51,66,67]. rOat1-mediated transport has been characterized by *trans*-stimulation. An outward concentration gradient of substrates, including dicarboxylates preloaded by preincubation or via sodium-dicarboxylate cotransporter, stimulates rOat1-mediated transport, suggesting that rOat1 functions as an exchanger [66,67]. rOat2 was found by a database-search and registered as a novel-liver specific transporter (NLT) [68,69]. Functional expression in *X. laevis* oocytes revealed that NLT transports α-ketoglutarate, PGE_2, PAH, methotrexate and acetylsalicylate [69]. When expressed in LLC-PK1 cells as a host, it transports indomethacin, PGE2, and nucleoside analogs, such as azidodeoxythymidine and dideoxycytidine, although specific uptake of methotrexate and PAH was not detected [70].

3.2.2. Organic cation transporter (Oct/OCT: SLC22A)

Organic cation transporters (Oct/OCT) are multispecific facilitative transporters of hydrophilic and small organic cations. Review articles of the Oct/OCT family are available in Refs. [10,11,13,21]. Three isoforms (Oct1/OCT1–Oct3/OCT3) have been isolated from rodents and in human. The Oct isoform expressed in the CP is controversial. RT-PCR analysis using cDNA from rat CP as a template revealed expression of rOct2 (*Slc22a2*) and rOct3 (*Slc22a3*) mRNA, but not rOct1 (*Slc22a1*) mRNA, in the CP [71]. However, mRNA quantification by Choudhuri et al. [26] revealed the low-level expression of rOct1 and rOct3 in the rat CP, and the expression level of Oct2 mRNA was below the detection limit. rOct1 was initially cloned from the rabbit by expression cloning using *X. laevis* oocytes [72]. Subsequently other isofoms, rOct2 and rOct3, have been cloned from kidney and placenta cDNA libraries using homology screening [73,74]. rOct1 is expressed abundantly in the kidney, liver and, to a lesser extent, in the intestine [72], while hOCT1 is abundantly expressed in the liver [75,76]. rOct2/hOCT2 is expressed predominantly in the kidney [73,75]. rOct3 has a ubiquitous expression profile and is relatively abundant in the placenta [74].

The Oct1-mediated uptake is characterized by its membrane voltage dependence [72]. For example, an intracellular negative membrane voltage facilitates rOct1-mediated transport of hydrophilic organic cations and substitution of Na^+ for K^+ reduces the transport activity, due to depolarization of the membrane voltage [72]. Oct/OCT-mediated uptake is reduced under conditions that cause depolarization of the membrane voltage, such as substitution of K^+ for Na^+, Ba^{2+} and ouabain treatment, as well as an extracellular acidic pH [10,11,13,21]. It has been shown that members of the Oct/OCT family have a similar substrate specificity, i.e. small and hydrophilic organic cations, such as tetraethylammonium (TEA) and *N*-methylnicotineamide (NMN), although rOct3 exhibits a relatively lower affinity for TEA compared with rOct1 and rOct2 [10,11,13,21,74,77,78]. The membrane localization of rOct1, rOct2 and rOct3 in the CP remains unknown. Sweet et al. [71] produced a chimeric protein of rOct2-GFP and transfected it to rat isolated CP. The fluorescence associated with the chimeric protein was localized at the BBM of the CP, suggesting the apical localization of endogenous rOct2 in the CP, if it is expressed in the CP.

Oct1, Oct2 and Oct3, as well as Oct1/Oct2 double knockout mice have been developed [79–81]. These mouse strains are healthy and exhibit no significant physiological abnormalities. No functional characterization of the organic cation transport in the CP has been carried out using these animals. These mice will allow us to investigate the role of Oct isoforms in the transport of organic cation in the CP.

3.2.3. OCTN (SLC22A)

Three isoforms (Octn1–Octn3) have been isolated in rodents, while two isoforms (OCTN1 and OCTN2) have been isolated in humans. Review articles of the Octn/OCTN family are available in Refs. [14,51,53]. Choudhuri et al. [26] demonstrated abundant expression of rOctn2 (*Slc22a5*) in the CP and, to a lesser extent, rOctn1 (*Slc22a4*), while the expression of rOctn3 remains to be quantified. Both hOCTN1 (*SLC22A4*) and hOCTN2 (*SLC22A5*) show ubiquitous tissue distribution [82,83] Octn2/OCTN2 has been characterized as a sodium-dependent carnitine transporter [83,84], although it also transports TEA [85]. Octn2 is hereditarily deficient in the juvenile visceral steatosis (*jvs*) mouse [86], a model animal of primary systemic carnitine deficiency (OMIM 212140). A single nucleotide mutation (TG) causes substitution of Leu by Arg at codon 352 leading to a loss of transport function [86]. Lack of Octn2 causes marked reduction in the renal reabsorption of carnitine and the tissue distribution in the heart, liver and brain capillaries [87–89]. Furthermore, pharmacokinetic studies in jvs mouse suggested an involvement of Octn2 in the tubular secretion of TEA [90]. The renal clearance of TEA was significantly decreased in the jvs mouse compared with its corresponding wild-type mice, while that of an organic anion, cefazolin [90]. Mutations, causing functional loss, have been found in patients suffering from primary systemic carnitine deficiency [86].

OCTN1 has been considered to be a proton/organic cation exchanger since an acidic pH stimulates the efflux of TEA in OCTN1-expressing HEK293 cells [82]. The substrates of OCTN1 include organic cations, such as pyrilamine, quinidine and verapamil, as well as carnitine. In contrast to the transport of cationic compounds by hOCTN1, hOCTN1-mediated carnitine uptake shows sodium dependency [82]. The transport activity of carnitine by mOctn1 is much lower than that by mOctn2 [85].

3.3. Peptide transporter (PEPT; SLC15A)

Peptide transporters are classified within the gene superfamily of solute carriers (SLC) as the *SLC15A* gene family. In rat CP, PEPT2 (*Slc15a2*), but not PEPT1 (*Slc15a1*), has been identified at the BBM of CPE [91]. The details of this transporter are summarized in another review of this issue. Briefly, PEPT2 accepts di- and tripeptides, as well as peptide-mimetic drugs, such as β-lactam antibiotics containing an α-amino group, and angiotensin-converting enzyme inhibitors are also substrates of PEPT2 [92–96]. The functional role of PEPT2 in the CP has been shown using the Pept2 knockout mouse [97]. The cellular accumulation of glycylsarcosine and cefadroxil, typical ligands of PEPT2, by the isolated CP is considerably reduced in Pept2 knockout mice [97,98].

3.4. ABC transporters

ABC transporters are characterized by the cytoplasmically located ATP-binding cassette acting as a catalytic domain for ATP hydrolysis and by the unidirectional efflux to the outside of the cells. This section focuses on the molecular characterization of multidrug resistance-associated proteins (MRPs) and P-glycoprotein (P-gp).

3.4.1. Multidrug resistance-associated protein (MRP; ABCC)

MRPs have been classified within the gene superfamily of ABCC and eight different ABCC proteins (MRP1–8) have been cloned [99–102]. Review articles of the Mrp/MRP family are available in Refs. [103–106].

As far as the Mrp/MRP members are concerned, RT-PCR and Western blot analyses have revealed the expression of rMrp1 (*Abcc1*) in the CP where it is localized on the basolateral membrane of the CPE [24,107,108]. MRP1 has been found to be present as a protein overexpressed in the doxorubicin-selected lung cancer cell line H69AR, which confers multidrug resistance to tumor cells [109]. The mRNA of human MRP1 (*ABCC1*) encodes 1531 amino acids with an apparent molecular weight of 190 kDa and 17 transmembrane domains with two cytoplasmically located ATP-binding cassettes [109]. MPR1 has a broad substrate specificity including amphipathic glucuronide and glutathione conjugates [110,111]. In the presence of glutathione, hMRP1 can accept vincristine and estrone sulfate as substrates [106,112].

Taking the unidirectional transport as being directed from inside the cells to the outside, Mrp1 is a candidate transporter for basolateral excretion of its substrates, including amphipathic organic anions in

the CP. In accordance with this hypothesis, the CSF concentration of etoposide is significantly increased in triple knockout mice (Mrp1/Mdr1a/Mdr1b knockout mouse) compared with that in double knockout mice (Mdr1a/Mdr1b knockout mouse), although there is no difference in the plasma and brain concentrations of etoposide between double and triple knockout mice [113]. However, Lee et al. [114] reported only a minimal difference in the CSF concentration of E217βG and dinitrophenyl-*S*-glutathione after i.c.v. administration between wild-type and mMrp1 knockout mice, suggesting that Mrp1 may not play a major role in the efflux of organic anions across the BLM of the CP.

Quantification of Mrp mRNAs (mMrp1–mMrp6) has revealed abundant expression of mMrp4 (*Abcc4*) and mMrp5 (*Abcc5*) in the mouse CP [26,114]. hMRP4 (*ABCC4*) and hMRP5 (*ABCC5*) mRNAs encode 1325 and 1437 amino acid proteins, respectively, with 12 putative transmembrane domains. The apparent molecular weight of hMRP4/rMrp4 is approximately 170 kDa in the BBM from the kidney [115]. The substrates of hMRP4 include nucleoside analogs and cyclic nucleotides, as well as amphipathic organic anions, such as E217βG, dehydroepiandrosterone sulfate, methotrexate and prostaglandins [115–120], whereas cAMP, cGMP, 6-mercaptopurine and adefovir are known substrates of hMRP5 [121,122]. Further studies are necessary to reveal their functional role in the CP.

3.4.2. P-glycoprotein (ABCB1)

P-glycoprotein (P-gp: *ABCB1*) was originally found as an overexpressed protein at the plasma membrane of multidrug resistant tumor cells. The mRNA of human MDR1 encodes 1280 amino acids with an apparent molecular weight of 140–170 kDa and 12 transmembrane domains with two cytoplasmically located ATP-binding cassettes. In rodents, two isoforms, namely, Mdr1a (*Abcb4*) and Mdr1b (*Abcb1*), correspond to the human ortholog (MDR1). Mdr1a plays a central role in efflux transport at the brain capillary and small intestine [123,124]. P-gp has a broad substrate specificity including hydrophobic neutral or cationic compounds, fexofenadine and E217βG [125–128]. The importance of P-gp is well recognized in the brain capillaries [6,7,103,124,129–131]. Rao et al. [108] demonstrated its expression in the CP by Western blotting. However, the signals detected by anti-P-gp antibody (C219) shows punctate or granular staining patterns at the subapical region of the primary cultured CPE, suggesting that it is confined to the vesicular compartment [108]. Whether P-gp plays a role as one of the detoxification mechanisms in the CP remains to be elucidated.

4. Efflux transport mechanisms for organic anions in the choroid plexus

The uptake mechanisms for organic anions at the brush border surface of the CP can be subdivided into two groups in terms of substrate specificity: One for amphipathic organic anions, such as taurocholate, E217βG and estrone sulfate, and the other for hydrophilic and small organic anions, such as PAH and benzylpenicillin (Fig. 1). These two systems have similar characteristics to the hepatobiliary and urinary transport systems for organic anions, respectively, and are primarily accounted for by the Oatp/OATP and Oat/OAT families.

4.1. Amphipathic organic anions

E217βG shows rapid elimination from the CSF compared with the CSF turnover rate (represented by the elimination of inulin). The CSF elimination clearance of E217βG is 12-fold greater than that of inulin (76 and 5.9 μl/min/rat, respectively) (Fig. 2). Similarly, estrone sulfate is rapidly eliminated from the CSF after i.c.v. administration [132]. According to the initial characterization by Nishino et al. [107], a saturable component accounts for part of the total uptake of E217βG and taurocholate by the isolated CP (~40% of the total uptake). The uptake is inhibited by probenecid and FCCP treatment causing a reduction in the intracellular ATP level, which reduces the accumulation of E217βG by the isolated rat CP, suggesting that the uptake process requires energy [107]. A second report by Kusuhara et al. [25] showed that a saturable component accounts for a major part of the total uptake of E217βG by the isolated rat CP with K_m values (55 μM) 16-fold greater than those previously reported (3.4 μM). The transport activity of TCA by the isolated rat CP was similar to that of E217βG (Fig. 3) and is saturable with a K_m value

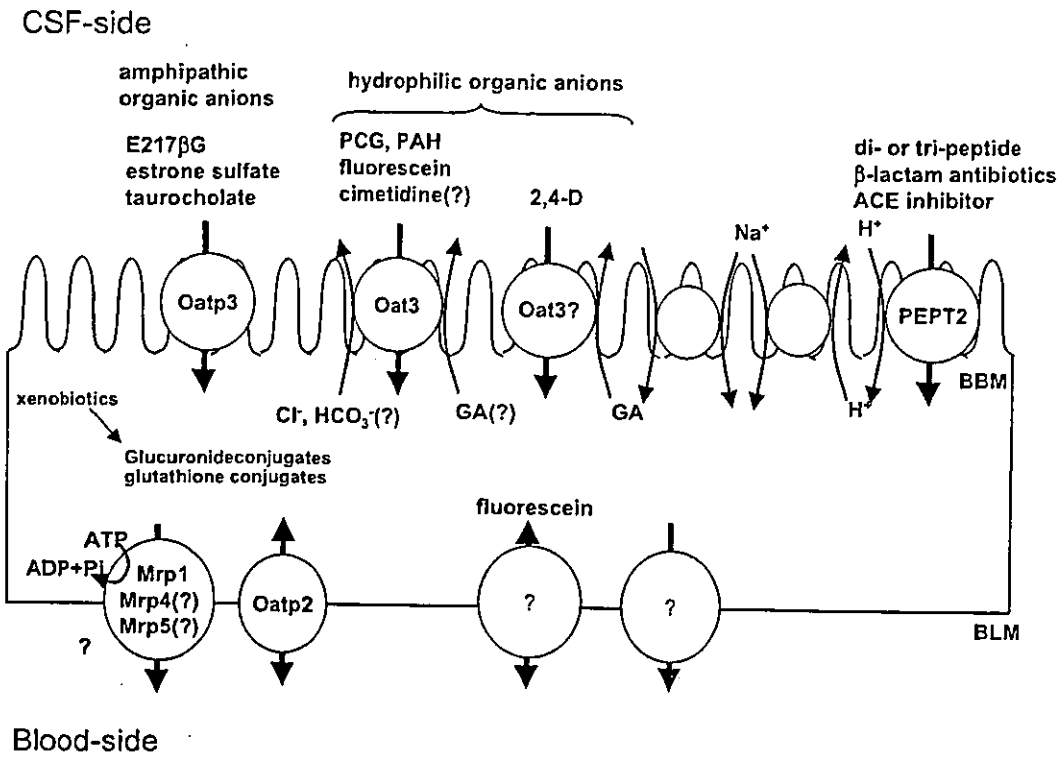

Fig. 1. Schematic diagram of the efflux transport systems for organic anions in the CP. The uptake of amphipathic organic anions, such as E217βG, taurocholate and estrone sulfate, at the BBM is mediated by organic anion-transporting polypeptide 3 (Oatp3). That of hydrophilic organic anions, such as benzylpenicillin (PCG), fluorescein and PAH, is mediated by organic anion transporter 3 (Oat3). The uptake mechanism for 2,4-dichlorophenoxyacetate (2,4-D) is unknown, but is mediated by the exchange of intracellular dicarboxylate (GA; glutarate). Peptide transporter 2 (PEPT2) may be involved in the uptake of β-lactam antibiotics and angiotensin-converting enzyme (ACE) inhibitors with an α-amino group, as well as di- and tripeptides. The basolateral excretion mechanisms for organic anions have not been fully elucidated. Mrp1 has been a candidate transporter, but its contribution to the efflux of amphipathic-conjugated metabolites remains controversial. Oatp2 and other ABC transporters, such as Mrp4 and Mrp5, are alternative candidate transporters. In addition, a membrane voltage-dependent efflux transport system has been suggested to be located on the basolateral membrane.

(116 μM), comparable with its K_i value for E217βG uptake by the isolated CP (124 μM) [25]. This suggests that they share the same uptake mechanism at the BBM. The K_m value of E217βG determined in the isolated CP is very close to that determined in oocytes expressing rOatp3 [32], but greater than that determined in rOatp3-expressed LLC-PK1 cells [25]. The spectrum of inhibitors, e.g. corticosterone, indomethacin, probenecid, diclofenac, estrone sulfate and quinine, for the uptake of E217βG by LLC-PK1-expressing rOatp3 and isolated CP is similar, although the absolute values of their K_is are not identical [25]. Since the effect of benzylpenicillin is minimal even at a concentration sufficient to saturate its own uptake by the isolated CP, the uptake of these two organic anions is mediated by different mechanisms at the BBM of the CP [25,107]. Although E217βG is a substrate of rOat3 [61], the minimal inhibition by benzylpenicillin indicates the minor contribution of rOat3 to the uptake of E217βG by the isolated rat CP. This is reasonable taking into consideration the transport activities of benzylpenicillin and E217βG in the CP and LLC-PK1 cells expressing rOat3. Their transport activities are similar in LLC-PK1 cells expressing rOat3 [55,61], whereas the uptake of E217βG by the isolated CP is fivefold greater than that of benzylpenicillin (Fig. 3).

Kitazawa et al. [132] have shown significant accumulation of estrone sulfate by the isolated rat CP, which is saturable with a K_m value of 18 μM. As observed for the uptake of E217βG, reduction of the intracellular ATP level during treatment of the CP with 2,4-dinitrophenol (metabolic inhibitor) and rotenone (inhibitor of mitochondrial respiration) markedly reduces the uptake of estrone sulfate. Amphipathic

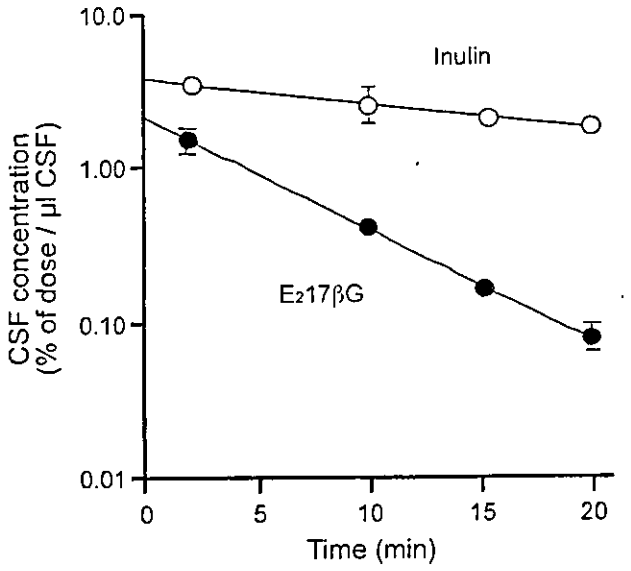

Fig. 2. The CSF concentration–time profiles of E217βG after intracerebroventricular administration in rats. Rats were given [^{3}H]E217βG (●; 0.38 µCi/rat) and [^{14}C]inulin (○; 0.02 µCi/rat) by i.c.v. administration and the cisternal CSF concentration of each compound was determined. Each point and vertical bar represents the mean±S.E. of three independent experiments. The solid line is the regression line. Taken from Nishino et al. [107].

organic anions, such as dehydroepiandrosterone sulfate, taurocholate and cholate inhibit the uptake significantly, whereas the effect of PAH and digoxin is minimal. Taking into consideration the localization and substrate specificity, rOatp3 is a candidate for the uptake of amphipathic organic anions.

To carry out efficient elimination from the CSF, the transporter will be involved in excretion across the BLM of the CPE. Strazielle and Ghersi-Egea [4] demonstrated asymmetrical efflux transport of 1-naphthol-17β-glucuronide in primary cultured rat CPE. Incubation of 1-naphthol with cultured cells produces the glucuronide conjugate intracellularly and the cumulative amount of intracellularly formed 1-naphthol-17β-glucuronide excreted into the basal side was 2.6-fold greater than that into the apical side. As described previously in Section 3.4.1, Mrp1 is the candidate transporter for the basolateral excretion of amphipathic organic anions. However, Lee et al. [114] showed comparable CSF concentrations of E217βG and 2,4-dinitrophenyl-glutathione after i.c.v. administration to the Mrp1 knockout mouse

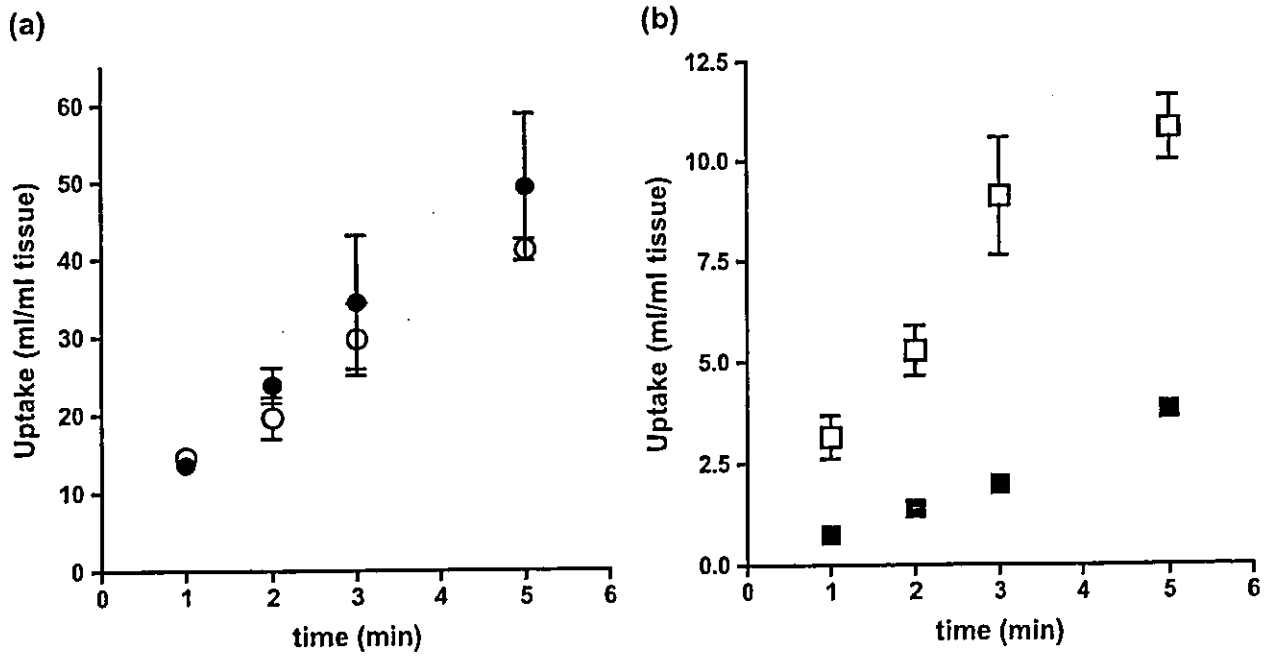

Fig. 3. Time profiles of the uptake of organic anions by the isolated rat CP. The CP was isolated from the lateral ventricles and the uptake of amphipathic and hydrophilic organic anions (panels a and b, respectively) by the isolated CP was determined by a centrifugal filtration method. The tissue-to-medium concentration ratio was calculated using [^{14}C]urea (panel a) or [^{3}H]water (panel b) as a cell water space marker and a correction was made for the adherent water space. (a) [^{3}H]E217βG (●; 0.01 µM), [^{3}H]taurocholate (○; 0.15 µM). (b) [^{14}C]benzylpenicillin (□; 0.2 µM) and [^{14}C]PAH (■; 0.2 µM). Taken from Kusuhara et al. [25] (panel a) and Nagata et al. [55] (panel b).

and the corresponding wild-type mouse. Another efflux mechanism may play a major role in the excretion of amphipathic organic anions across the BLM of the CP. According to the mRNA quantification, Mrp4 and Mrp5 may be alternative candidates [26,114]. Further studies are required to reveal their membrane localization in the CP and contribution to efflux transport via the CP.

4.2. Hydrophilic organic anions

In vivo kinetic analyses revealed the presence of a saturable elimination mechanism for benzylpenicillin in the ventricles [20,133]. Ogawa et al. [20] compared the kinetic parameters obtained in vivo using i.c.v. administration and in vitro using isolated rat CP. They found that the in vitro kinetic parameters (K_m 58 μM and V_{max} 504 pmol/min/rat) were comparable with those in vivo (K_m 43 μM and V_{max} 620 pmol/min/rat), indicating that the saturable efflux of benzylpenicillin in the ventricles is due to the uptake mechanism at the BBM of the CP [20]. This is also supported by a clear 1:1 correlation among the K_i values of probenecid and various β-lactam antibiotics for the efflux of benzylpenicillin from the CSF and for the uptake of benzylpenicillin by the isolated CP [20]. Hakvoort et al. [134] demonstrated that benzylpenicillin is accumulated on the basal side of the porcine CPE cultured on a porous membrane (Table 2). Similarly, fluorescein, phenol red, and riboflavin are accumulated in the basal compartment and this process is competitively inhibited by benzylpenicillin (Table 2) [134]. Mutual inhibition analyses have suggested multispecificity of the transporter for benzylpenicillin uptake at the BBM of the CP, which includes cefodizime (β-lactam antibiotic) [135], fleroxacin (quinolone antibiotic) [136] and PAH [55]. In addition to these compounds, a variety of β-lactam antibiotics have an inhibitory effect with K_i values ranging from 10 μM to 5.9 mM depending on their chemical structures [135,137]. Thus, it is likely that the transporter responsible for the benzylpenicillin uptake also plays a major role in regulating the CSF concentration of β-lactam antibiotics together with PEPT2 [98,138,139].

Table 2
Kinetic data of the investigated active transport systems in the primary cultured porcine choroid epithelial cells

Substrate	Transport direction	K_m [μM]	V_{max} [nmol/cm^2 h]
Ascorbic acid	b⇒a	67±12	3.91±0.29
myo-Inosipol	b⇒a	117±9	1.65±0.05
Penicillin G	a⇒b	107±8	1.82±0.05
Fluorescein	a⇒b	22±1.5	1.92±0.05
+400 μM Penicillin G		108±21	1.32±0.18
Phenol red	a⇒b	68±2.9	3.01±0.06
+400 μM Penicillin G		326±18	3.50±0.12
+20 μM Penicillin		340±23	2.52±0.12
Riboflavin	a⇒b	78±4	1.84±0.05
+400 μM Penicillin G		217±42	2.16±0.28

a: apical; b: basolateral.
Taken from Hakvoort et al. [134].

Suzuki et al. [137,140] investigated the driving force for the uptake of benzylpenicillin by the isolated CP. The uptake was markedly reduced by metabolic inhibitors, such as 2,4-dinitrophenol and KCN, suggesting the involvement of active transport [137]. Substitution of mannitol, Tris or *N*-methyl-D-glucamine, but not choline, for Na^+ slightly reduced the uptake to 70–80% of the control value, but ouabain, a Na^+K^+ ATPase inhibitor, did not affect the uptake [137]. Thus, benzylpenicillin uptake does not require an inward Na^+ concentration gradient. Whether benzylpenicillin uptake coupled to the export of intracellular anions was investigated using ATP-depleted CP, which was produced by incubating the isolated CP with 25 μM rotenone for 20 min, the intracellular ATP content was reduced from 27 to 0.97 nmol/mg protein [140]. The ATP-depleted choroid plexus has been incubated in the presence of anions, such as Cl^-, HCO_3^-, SCN^- and SO_4^{2-}, for their intracellular accumulation and subsequently transferred to the buffer without the anion to produce an outward-directed concentration gradient [140]. The uptake of benzylpenicillin was greater in the CP preloaded with Cl^- than in the CP preloaded with gluconate and the peak uptake in the presence of the Cl^- gradient was greater than that under equilibrium conditions [140]. Apart from Cl^-, the uptake was stimulated by the outwardly directed gradient of HCO_3^- and, to a lesser extent, by SCN^-. These anions are candidates for the driving force behind benzylpenicillin uptake into the choroid plexus.

As described previously, RT-PCR has detected the expression of rOat1, rOat2 and rOat3 mRNA in rat CP [54]. Especially, rOat3 has been shown to be expressed at the brush border surface of the rat CP.

Nagata et al. [55] investigated the uptake of PAH and benzylpenicillin as probe compounds for rOat1 and rOat3, respectively, by the isolated rat CP and compared their kinetic parameters (Fig. 4). Significant accumulation of PAH was observed in the isolated rat CP, but the transport activity was four-fold less than that of benzylpenicillin (Fig. 3) [55]. The K_m value of PAH was very close to the K_i value for benzylpenicillin uptake and vice versa. The inhibitors including cimetidine and E217βG, which do not affect rOat1-mediated transport, showed similar K_i values for PAH and benzylpenicillin uptake by isolated CP (Fig. 4). These results suggest that they share the same uptake mechanism at the brush border surface of the CPE. Furthermore, the K_i values for the inhibitors of benzylpenicillin uptake by isolated CP were comparable with those for rOat3 (Fig. 4). These kinetic results suggest that rOat3 plays a major role in the uptake of PAH and benzylpenicillin at the BBM of the CP. In addition, a marked reduction in the cellular accumulation of fluorescein in the isolated CP from the mOat3 knockout mouse [54] supports the idea that rOat3 is the likeliest candidate for the uptake of hydrophilic organic anions in the CP. Involvement of rOat3 has also been suggested in the uptake of a nucleoside analog, zidovudine [141]. The apical-to-basal transport across the primary cultured CPE, corresponding to the efflux from the CSF, of zidovudine, didanosine and lamivudine is greater than that in the opposite direction. The apical-to-basal transport of ziduvudine is saturable, and inhibited by 2,4-dichlorophenoxyacetate and benzylpenicillin [141].

The driving force for rOat3-mediated transport is considered to be an outward concentration gradient of dicarboxylate as described in Section 3.2.1. Similar transport properties were observed for the uptake of 2,4-dichlorophenoxylacetate (2,4-D) by the brush border surface of the CP. Pritchard et al. [142] clearly showed that extracellular or -vesicular glutarate stimulated the uptake of 2,4-D by the isolated CP and BBMV in the presence of an inward Na^+ concentration gradient (Fig. 5). Intravesicular glutarate, preloaded into the vesicles prior to the uptake experiment, could also stimulate the uptake of 2,4-D, suggesting the involvement of an exchanger for 2,4-D

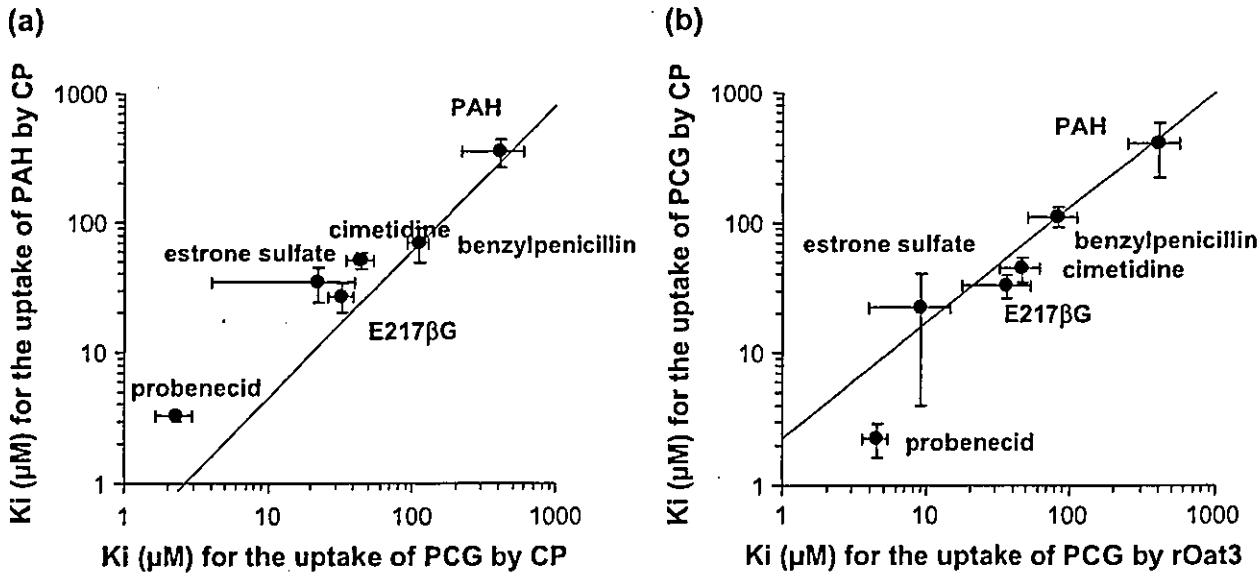

Fig. 4. Relationship between the K_m and K_i values for the uptake of PAH and benzylpenicillin by the CP, as well as the uptake of benzylpenicillin by the CP and rOat3. Correlation between the K_m and K_i values for the uptake of benzylpenicillin and PAH by the isolated rat CP (a), as well as those for the uptake of benzylpenicillin by the isolated rat CP and rOat3-expressing cells (b). The solid lines represent the regression line of the K_m and K_i values for the uptake of PAH and benzylpenicillin by the isolated rat CP (a; r=0.956, p<0.01), and the uptake of benzylpenicillin by the isolated rat CP and by rOat3 (b; r=0.985, p<0.01). Panel a suggests that benzylpenicillin and PAH share the uptake mechanism at the brush border surface of the CP. The K_m and K_i values for benzylpenicillin uptake by the isolated rat CP were comparable to those found in rOat3-expressing cells, suggesting that rOat3 is responsible for the uptake of benzylpenicillin by the isolated rat CP. Taken from Nagata et al. [55].